Fall 2006

Inverse solid-liquid fluidization of aerogel granules and its application in removing oil from water

Gaurav Babubhai Patel
New Jersey Institute of Technology

ABSTRACT

INVERSE SOLID-LIQUID FLUIDIZATION OF AEROGEL GRANULES AND ITS APPLICATION IN REMOVING OIL FROM WATER

by
Gaurav Babubhai Patel

Fluidization is a very well known unit operation used in the chemical industry for various purposes. Inverse solid-liquid fluidization, where the solid particles to be fluidized are less dense than the fluid, is one of the several different kinds of fluidization being studied for its potential in industrial applications. The present work focuses on finding the hydrodynamic characteristics (minimum fluidization velocity, bed expansion and pressure drop) of an inverse fluidized bed of aerogel granules and using this system to remove oil from an oil-water mixture. The solid particles employed for this study are low density (100 kg/m^3) surface treated hydrophobic aerogel (Nanogel®) granules of size in the range of 0.5 to 2.3 mm. These particles are highly porous characterized by a nanosized pore structure and a very high surface area. Since their density is lower than water, they are fluidized downward in a solid-liquid inverse fluidized bed column.

In this work, a constant flow of an oil-water mixture is passed through an inverse fluidized bed of aerogel granules. The oil concentration was determined by measuring the Chemical Oxygen Demand (COD) using a colorimeter. Once the aerogel granules are saturated, they were entrained from the fluidized bed, and separated from the clean stream of water with a fibrous filter.

INVERSE SOLID-LIQUID FLUIDIZATION OF AEROGEL GRANULES AND ITS APPLICATION IN REMOVING OIL FROM WATER

by
Gaurav Babubhai Patel

A Thesis
Submitted to the Faculty of
New Jersey Institute of Technology
In Partial Fulfillment of the Requirements for the Degree of
Master of Science in Chemical Engineering

Otto H. York Department of Chemical Engineering

January 2007

APPROVAL PAGE

INVERSE SOLID-LIQUID FLUIDIZATION OF AEROGEL GRANULES AND ITS APPLICATION IN REMOVING OIL FROM WATER

Gaurav Babubhai Patel

Dr. Robert Pfeffer, Thesis Advisor — Date
Distinguished Professor of Chemical Engineering (Emeritus), NJIT
Distinguished Research Professor, NJCEP

Dr. Rajesh N. Dave, Committee Member — Date
Distinguished Professor of Chemical Engineering, NJIT

Dr. Michael C.Y. Huang, Committee Member — Date
Assistant Professor of Chemical Engineering, NJIT

BIOGRAPHICAL SKETCH

Author: Gaurav Babubhai Patel

Degree: Master of Science

Date: January 2007

Undergraduate and Graduate Education:

- Master of Science in Chemical Engineering,
  New Jersey Institute of Technology, Newark, NJ, 2007

- Bachelor of Engineering in Chemical Engineering,
  G.H. Patel College of Engineering and Technology, Gujarat, India, 2003

Major: Chemical Engineering

Publications:

J. Quevedo, G. Patel, R. Pfeffer. "Removal of Oil from Water by Inverse Fluidization of Aerogels," *in preparation.*

J. Quevedo, G. Patel, R.Pfeffer, R. Dave. "Filtration of Submicron Particles by Using Agglomerates of Nanoparticles as Filter Media," *in preparation.*

J. Quevedo, G. Patel, R. Pfeffer, "Residence Time Distribution Study of Packed and Fluidized Bed of Agglomerates of Nanoparticles," *in preparation.*

This thesis is dedicated to

my Mom (Madhuben B. Patel) and Dad (Babubhai A. Patel).

ACKNOWLEDGMENT

I feel proud to have Dr. Robert Pfeffer as my Thesis Advisor. I greatly appreciate his support for the entire work as well as my graduate studies. His guidance and knowledge was a great help in the process of developing this work. He also gave me an opportunity to work on other interesting projects that he and his students are involved in.

I express my gratitude to Dr. Rajesh Dave for being a member of the committee. He was very kind to give me proper advice for my research work.

I thank Dr. Michael Huang for not only being a committee member but also for providing me with his knowledge, encouragement and time.

I would also like to thank the National Science Foundation (NER award) and the Cabot Corporation for their financial support to this project.

I would like to give my special thanks to Jose Quevedo for working with me, guiding me, and sharing his knowledge and experience, without which it would have been difficult to finish the research properly.

I should not forget to thank my colleagues, Daniel Lepek, and Ayokunle Omosebi for their kind assistance in this work. I would also like to thanks the Chemical Engineering Department of NJIT for providing the necessary support and advice. And I also thank Cabot Corporation for providing the necessary particulate materials used in the experiments.

TABLE OF CONTENTS

Chapter		Page
1	INTRODUCTION	1
	1.1 Objectives of the Present Study	1
	1.2 Organization of this Thesis	1
	1.3 Overview	2
	1.4 Silica Aerogel	4
	1.5 Previous Studies about Inverse Fluidization	5
	1.6 Current Oil Removal Techniques	18
2	INVERSE FLUIDIZATION OF NANOGEL	33
	2.1 Introduction	33
	2.2 Experimental Setup and Procedure	34
	2.3 Results and Discussion	38
	2.3.1 Determination of the Granule Density (ρ_p) and the Internal Porosity (ε_p) of the Granule from Experimental Data	45
	2.3.2 Richardson-Zaki Analysis to Find the Terminal Velocity (U_t) and to Estimate the Granule Size (d_p)	49
	2.3.3 Comparison of Experimental and Calculated Minimum Fluidization Velocity	53

TABLE OF CONTENTS
(Continued)

Chapter	Page
3 OIL REMOVAL USING INVERSE FLUIDIZED BED OF NANOGEL.....	56
3.1 Introduction	56
3.2 Experimental Setup and Procedure	59
3.3 Results and Discussion.....	61
4 CONCLUSIONS AND RECOMMENDATIONS FOR FUTURE STUDY	76
REFERENCES	79

LIST OF TABLES

Table		Page
1.1	Equations Classified According to the Range of Archimedes Number.....	14
1.2	Overview of Existing Water Treatment Processes for Oil Renoval.....	19
1.3	Comparison of Oil Removal Efficiencies of Vermiculite and Other Sorbents.....	28
1.4	Comparison of Adsorption Capacities of Hydrophobic Silica Aerogel and Granulated Activated Carbon	29
2.1	Calculation of the Granule Density and the Initial Void Fraction from Experimental Data	49
2.2	Richardson-Zaki Bed Expansion Parameters and Calculation of the Particle Size from Experimental Data	53
2.3	Comparison of the Experimental and Theoretical Minimum Fluidization Velocities	54

LIST OF FIGURES

Figure		Page
1.1	Translucent Aerogel (Cabot Nanogel®).....	4
1.2	Frictional pressure drop versus liquid superficial velocity	6
1.3	Bed height versus superficial velocity of liquid	7
1.4	Pressure drop for three-phase inverse fixed and fluidized beds of polyethylene beads	12
1.5	Comparison of experimental and predicted terminal velocities	16
1.6	Classification of oil-water mixtures according to droplet size and corresponding removal methods	20
1.7	A simple Oil Water Separator	21
1.8	The American Petroleum Institute (API) type separator perspective view...	22
1.9	The Spill Control type separator section view	22
1.10	Coalescing Plate type separator perspective view	23
1.11	The working of an Ultrafiltration membrane	25
1.12	A granular bed filter with Granular Activated Carbon as filter media.....	26
1.13	A typical example flow sheet of a filtration plant	31
2.1	Different stages of inverse fluidization by increasing the fluid velocity	33
2.2	Schematic diagram of the inverse fluidization experimental setup	35
2.3	Pressure drop across the empty column.....	39
2.4	A typical plot of the inverse fluidized bed pressure drop	39

LIST OF FIGURES
(Continued)

Figure		Page
2.5	Difference in U_{mf} and pressure drop due to sieving and not sieving the particles	40
2.6	A plot showing that U_{mf} does not change by changing the amount of granules	41
2.7	Change in U_{mf} with a change in granule size	42
2.8	Effect of entrainment on the bed pressure drop	43
2.9	Bed expansion with different amount of granules of the same size	44
2.10	Bed expansion with two different size of granules of comparable mass	45
2.11	Schematic of an aerogel granule with the forces acting on it	46
2.12	Relationship between the superficial velocity and the void fraction of inverse fluidized beds of aerogel granules of the type TLD 101	51
2.13	Relationship between the superficial velocity and the void fraction of inverse fluidized beds of aerogel granules of the type TLD 302	51
3.1	The four bottles contain 0, 1.5, 10, and 30% GAC/Aerogel composite respectively in a crude oil water mixture	58
3.2	Correlation between the oil concentration in water and COD levels measured by HACH DR/890 Colorimeter	60
3.3	Chemical oxygen demand (COD) vs. time of 56 grams of aerogel granules (TLD 302 and OGD 303) with sizes between 1.7 to 2.3 mm (large) and 0.5 to 0.85 mm(small) during removal of oil from water (0.28 g of oil/kg of water and fluid velocity of 0.0305 m/s)	63

LIST OF FIGURES
(Continued)

Figure		Page
3.4	Bed expansion vs. time of 56 grams of aerogel granules (TLD 302 and OGD 303) with sizes between 1.7 to 2.3 mm (large) and 0.5 to 0.85 mm(small) during removal of oil from water (0.28 g of oil/kg of water and fluid velocity of 0.0305 m/s)	64
3.5	Pressure drop across the inversely fluidized beds of aerogel during the removal of oil corresponding to Figures 3.3. Superficial flow velocity was kept constant at 0.0305 m/s	65
3.6	Chemical oxygen demand (COD) vs. time of 56 grams and 100 grams of aerogel granules (OGD 303) with sizes between 0.5 to 0.85 mm(small) during removal of oil from water (0.19 g of oil/kg of water and fluid velocity of 0.0305 m/s)	66
3.7	Inverse fluidized bed expansion as a function of time of 100 grams of aerogel granules (OGD 303) with sizes between 0.5 to 0.85 mm during removal of oil from water (0.19 g of oil/kg of water and fluid velocity of 0.0305 m/s)	67
3.8	Pressure drop across the inversely fluidized beds of aerogel during the removal of oil corresponding to Figures 3.6. Superficial flow velocity was kept constant at 0.0305 m/s	68
3.9	Chemical oxygen demand (COD) vs. time of 56 grams of aerogel granules (OGD 303) with sizes between 0.5 to 0.85 mm during removal of oil from water (0.17 g of oil/kg of water and 0.0248 m/s fluid velocity).....	68
3.10	Chemical oxygen demand (COD) vs. time of 56 grams of aerogel granules (OGD 303) with sizes between 0.5 to 0.85 mm during removal of oil from water (0.36 g of oil/kg of water and 0.0244 m/s fluid velocity).	69

LIST OF FIGURES
(Continued)

Figure **Page**

3.11 Inverse fluidized bed expansion vs. time of 56 grams of aerogel granules (OGD 303) with sizes between 0.5 to 0.85 mm during removal of oil from water corresponding to Figure 3.9 and 3.10..... 70

3.12 Pressure drop across the inversely fluidized beds of aerogel during the removal of oil corresponding to Figure 3.9 and 3.10. Superficial flow velocity was kept constant at 0.0244 m/s 70

3.13 Chemical oxygen demand (COD) vs. time of 56 grams of aerogel granules (TLD 101) with sizes between 0.5 to 0.85 mm during removal of oil from water (0.45 g of oil/kg of water) at two different velocities of 0.0107 m/s (low velocity) and 0.0183 m/s (high velocity) 71

3.14 Chemical oxygen demand (COD) as a function of time of 108 grams and 56 grams of aerogel granules (TLD 101) with sizes between 0.5 to 0.85 mm during removal of oil from water (0.47 g of oil/kg of water and 0.0102 m/s fluid velocity) 73

3.15 Chemical oxygen demand (COD) vs. time of 100 grams of aerogel granules (TLD 101) with sizes between 1.7 to 2.3 mm (large) and 0.5 – 0.85 mm (small) during removal of oil from water (0.4 g of oil/kg of water) 74

LIST OF SYMBOLS

A	cross-sectional area of the fluidized bed column, m
Ar	Archimedes number, nondimensional
C	effluent solute concentration, kg/m^3
C_0	influent solute concentration, kg/m^3
Cd	Drag coefficient, nondimensional
d	coefficient of effective diffusion, m^2/s
d*	dimensionless particle diameter
dp	diameter of particle, m
D_p	droplet diameter, m
D	diameter of fluidized bed column, m
D_l	liquid phase axial dispersion coefficient, cm^2/s
f	drag force function, nondimensional
F_g	gravity force, N
F_B	buoyancy force, N
F_D	drag force, N
Fr_{mf}	Froude number at minimum fluidization, nondimensional
g	gravitational acceleration, m/s^2
Ga	Galileo number, $d_p^3 g \rho_l^2 / \mu_l^2$, nondimensional
h	travel distance of droplet, m
H	fluidized bed height, m
H_0	static bed height, m

k	Thomas rate constant, $m^3/(s.gm)$
K	liquid-solid mass transfer coefficient, m/s
m	mass of the adsorbent, kg
m_p	mass of particles, kg
M	mass of the adsorbent used, kg
Mv	density number, $(\rho_l - \rho_s)^2/ \rho_l^2$, nondimensional
n	Richardson-Zaki exponent
N_D	Best number, (4/3)Ar, nondimensional
ΔP_{exp}	experimental differential pressure drop across the fluidized bed, N/m^2
q_0	maximum solid-phase concentration of the sorbed solute, kg/kg
Q	flow rate, m^3/s
Re	Reynolds number, nondimensional
Re_g	gas Reynolds number, $u_g d_p \rho_g/ \mu_g$, nondimensional
Re_{gmf0}	Reynolds number at minimum fludization for three-phase sytem with batch liquid, $u_{gmf0} d_p \rho_g/ \mu_g$, non dimensional
Re_{lmf}	Reynolds number at minimum fluidization for three phase system
Re_{lmf0}	Reynolds number at minimum fluidization for two phase system
R_{emf}	Reynolds number at minimum fluidization, nondimensional
Re_p	particle Reynolds number, nondimensional
Re_t	particle terminal Reynolds number, nondimensional
S	a constant describing the rate of adsorption, $kg/(g.s^{1/2})$
Sc	Schmidt number, $\mu_l/(\rho_l d)$, nondimensional
Sh	Sherwood number, Kdp/d, nondimensional
t	time, s

u_g	gas velocity, m/s
u_{gmf0}	superficial gas velocity at minimum fluidization for three-phase sytem with batch liquid, m/s
u*	dimensionless terminal velocity
U	superficial liquid velocity, m/s
U_i	settling velocity of granule at infinite dilution, m/s
U_{mf}	minimum fluidization velocity, m/s
U_t	terminal velocity of granule, m/s
V	throughput volume, m^3
V_b	total volume of the bed, m^3
V_{b0}	initial total volume of the bed, m^3
V_p	volume of the granule, m^3
V_ε	void volume of the bed, m^3
X	mass of the solute adsorbed to the solid, kg

Greek Letters

ε	void fraction of the bed, nondimensional
ε_l	liquid holdup, nondimensional
ε_{loc}	local void fraction, nondimensional
ε_p	internal porosity of the agglomerate, nondimensional
Φ	solid fraction of the bed, nondimensional
γ_r	relative conductivity, nondimensional
Γ	electrical conductance, ohm^{-1}
μ_g	viscosity of gas, $N.s/m^2$
μ_l	viscosity of liquid, $N.s/m^2$
ν	terminal velocity of oil droplet, m/s
ϑ	viscosity of the continuous phase, $N.s/m^2$
ρ^1	density of oil, kg/m^3
ρ_b	bulk density of the fluidized bed, kg/m^3
ρ_{b0}	initial bulk density of the fluidized bed, kg/m^3
ρ_g	density of gas, kg/m^3
ρ_l	density of liquid, kg/m^3
ρ_p	density of granule, kg/m^3
ρ_s	density of solid, kg/m^3

CHAPTER 1

INTRODUCTION

1.1 Objectives of the Present Study

This thesis work covers the inverse solid-liquid fluidization of aerogel granules and use of this process to remove oil droplets from water. The aerogel granules studied were Cabot Nanogel® (TLD 302, TLD101, and OGD 303) with different size ranges.

The fluidization behavior of the Nanogel® particles was observed and quantified in terms of available modeling concepts including the Richardson-Zaki model. The models are used to predict fluidization characteristics such as bed pressure drop and agglomerate size and these results are compared with the experimental data. The efficiency and capacity of the inverse fluidized bed of Nanogel® particles to remove oil from water is also examined and the behavior of these particles after absorption of oil on their surfaces is noted and explained.

1.2 Organization of this Thesis

This chapter is basically an overview of the objectives of this thesis. An introduction about the usefulness of both conventional and inverse fluidization for various industrial applications is given. The formation and fabrication of silica aerogels used in the experiments is recalled and their different properties and applications explained. Some pertinent studies regarding inverse fluidization found in the literature are described in detail. In the latter part of the chapter a number of conventional oil removal techniques are described, including some of the latest research on using some new adsorption media.

Chapter 2 describes in detail the concept of inverse fluidization. Some hydrodynamic parameters such as the terminal velocity of particles, minimum fluidization velocity, drag force, gravitational and buoyancy forces, and pressure drop, which determine the behavior of any fluidized bed, are studied. The Richardson-Zaki model is discussed and applied to the experimental data obtained from the inverse fluidized bed of Nanogel. This method has been used to predict the granule size and the granule density.

Chapter 3 describes the need to remove oil from wastewater. It also briefly mentions the usefulness of some adsorption media to remove oil from water. The possibility of using an inverse fluidized bed as a novel technique to remove oil is investigated. The experimental data are summarized in tables and plots and a discussion of the results obtained regarding the removal capacity and removal efficiency is presented.

Chapter 4 summarizes the overall conclusions derived from the experiments conducted and described in Chapter 2 and Chapter 3 and makes recommendations for some future work that needs to be done.

1.3 Overview

Fluidization is a phenomenon which has received widespread attention in terms of research and its application in industries for various purposes. Conventional industrial uses of fluidization include drying/humidifying of solid particles, catalytic cracking of hydrocarbons, coating and granulation of solid particles, adsorption of gas/liquid on the surface of solid particles, biological treatment of waste water, aerobic fermentation, etc. An interesting application of fluidization is a process for producing carbon nanotubes.

Thus, fluidization is commonly used where an interaction of fluid and solid particles in terms of momentum, heat and/or mass transfer is required.

Fluidization can be simply classified according to the continuous phase present in the fluidization column, as liquid phase or gas phase fluidization. In addition, there is also three phase (gas-liquid-solid) fluidization. The solid particles that are fluidized are basically fine powders whose primary particle size ranges from a few millimeters down to a few microns. Moreover, the solid particles may have a bulk density which is smaller or greater than the continuous phase in the column. If the particles have a bulk density greater than the continuous phase then, at the beginning of the fluidization, the particles remain at the bottom of the bed and they are fluidized upwards against gravity. But, if the particles have a density smaller than the fluid then they tend to stay at the top of the bed, so they have to be fluidized in the downward direction. This type of fluidization in which the flow of a liquid of higher density than the particles enters the column from the top, fluidizing the particles downwards in the direction of gravity, is called inverse fluidization. Advantages of both conventional and inverse fluidization include continuous operation, high rates of heat and mass transfer, high rates of chemical reaction, very good mixing between the particles, low pressure drop and adjustable bed voidage during fluidization. Inverse fluidization is also being extensively studied as a bio-reactor in waste water treatment plants and other biochemical processes where a constant biofilm thickness on the fluidizing particles is necessary.

In this dissertation, the hydrodynamic aspects of inverse fluidization of aerogels and the possibility of using these particles for removing oil from oil-water mixture were studied.

1.4 Silica Aerogel

The solid phase used in the fluidization experiments were silica aerogel granules (Cabot Nanogel®). Silica aerogels have low densities, large surface area and a high degree of porosity. Almost 85-99% of the bulk volume is the total pore volume of the particle and the pore size may lie in the range of 2-50nm. Figure 1.1 shows some photographs of the large (~2 mm) translucent aerogel granules with a magnified internal networked structure.

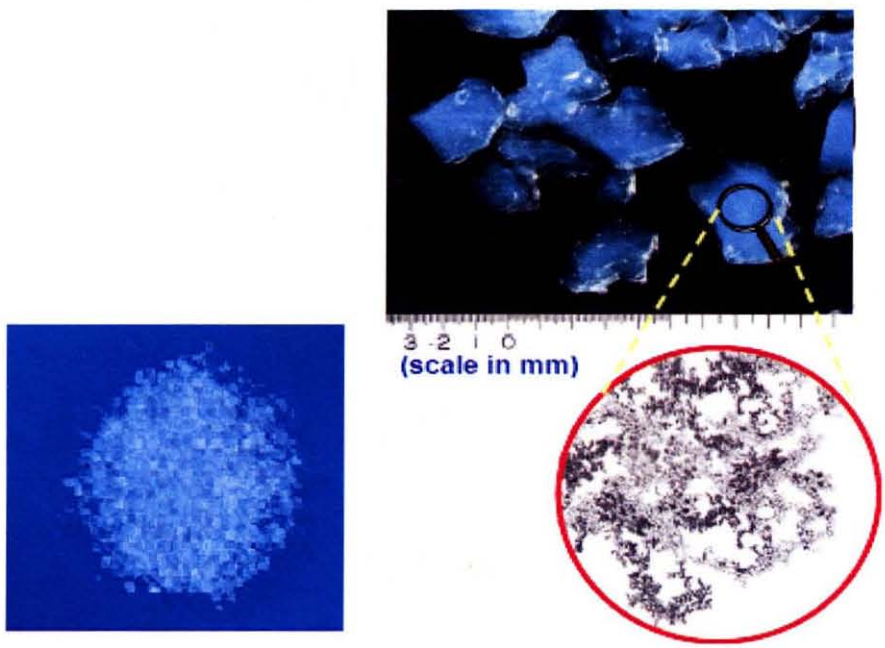

Figure 1.1 Translucent Aerogel (Cabot Nanogel®).

The method for the fabrication of these aerogels is described in US Patent 2,093,454; US Patent 2,188,007; and US Patent 2,249,767. An alkoxysilane, such as tetraethoxysilane, is mixed with water in an alcohol solution to prepare silica aerogel. An example of the balanced chemical equation for the formation of a silica gel from tetraethoxysilane is (Smirnova, 2002):

$$Si(OCH_2CH_3)_{4\ (liq.)} + 2H_2O_{\ (liq.)} = SiO_{2\ (solid)} + 4HOCH_2CH_{3\ (liq.)} \quad (1.1)$$

As hydrolysis and condensation reaction progress small silica particles are formed, and the reactive groups (either alkoxy or hydroxyl) on the surface of these particles interact with similar groups on a nearby particle forming links. These linkages result in a three-dimensional structure of silica particles which eventually convert the liquid sol into a semi-solid gel. The silica particles held by the linkages cannot dissociate from each other and the rest of the volume in the silica network is occupied by water and alcohol. The water and alcohol are removed from the network by replacing them with a pure solvent, like CO_2, and then applying heat and pressure to convert the liquid into a supercritical fluid. Then the pressure is reduced keeping the temperature above the critical temperature which forces the supercritical fluid to transition into a gas. This procedure avoids having the solvent to cross the liquid/vapor phase boundary which can generate capillary forces high enough to destroy the matrix of silica particles.

Silica aerogels such as Cabot Nanogel® have been studied in this research here because of their desirable properties of having an extremely high surface area and a very high porosity, which along with their hydrophobicity indicate that these aerogels can be used as an oil adsorbent.

1.5 Previous Studies about Inverse Fluidization

The Figure 1.2 shows the pressure drop across a bed of particles as a function of the flow velocity. It can be seen that as the flow of liquid through the bed of particles increases, the pressure drop rises steeply in the beginning because the flow has to pass through a

packed bed of particles. Due to the lower density of the particles, they tend to float on water because the buoyancy force dominates. The flow of liquid exerts a drag force that tries to balance the buoyancy force. When the velocity of liquid reaches to a point when the upward buoyancy force exerted on the floating particles is equal to the downward drag force plus the gravity force, the bed of particles is fluidized. This velocity is called the minimum fluidization velocity and at this point the expansion of bed begins.

There is another velocity called the entrainment velocity or the terminal velocity of the particles which is not shown in the Figure 1.2. When the velocity of the liquid increases to a point when the buoyancy force is no longer strong enough compared to the drag force plus the weight of the particle, the particles are entrained by the liquid and move out of the column. This is the entrainment velocity and it is important because it gives a design limit of the operating velocity of this system.

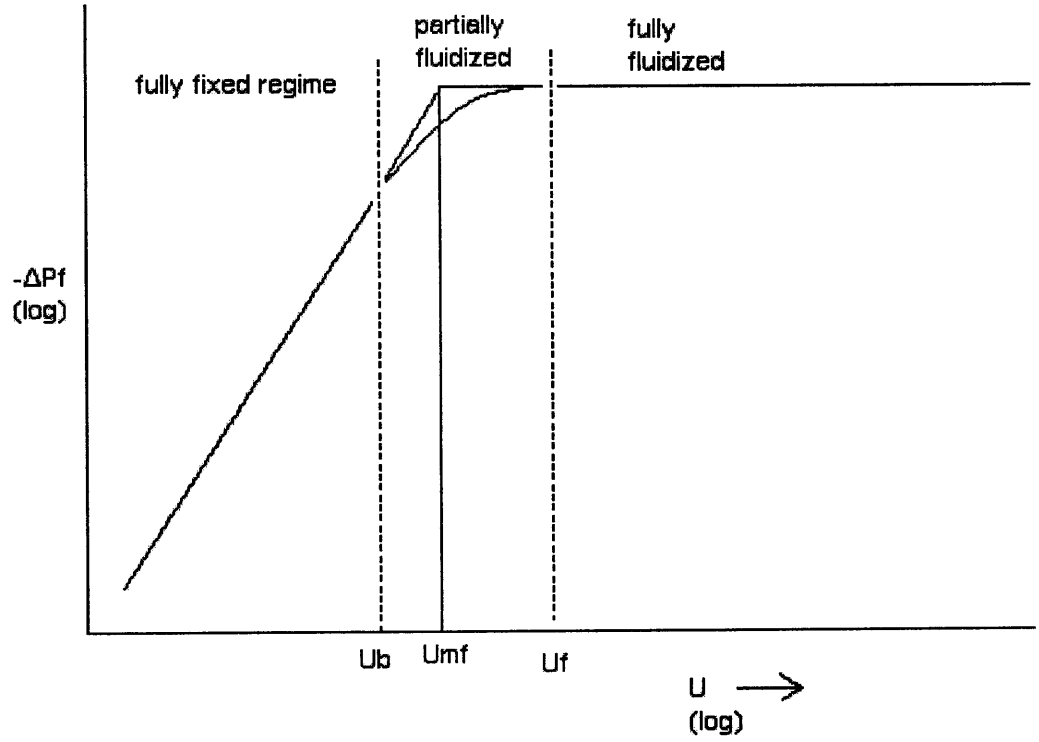

Figure 1.2 Frictional pressure drop versus liquid superficial velocity (Wen et al. 1966).

The Figure 1.3 shows the bed height as a function of the velocity of liquid. It can be seen that when the velocity reaches the minimum fluidization velocity the bed height starts increasing until the velocity reaches the point when the entire bed is entrained with the flow of liquid and exits the column. This velocity is important because it gives us the maximum value of velocity at which the fluidization can be operated.

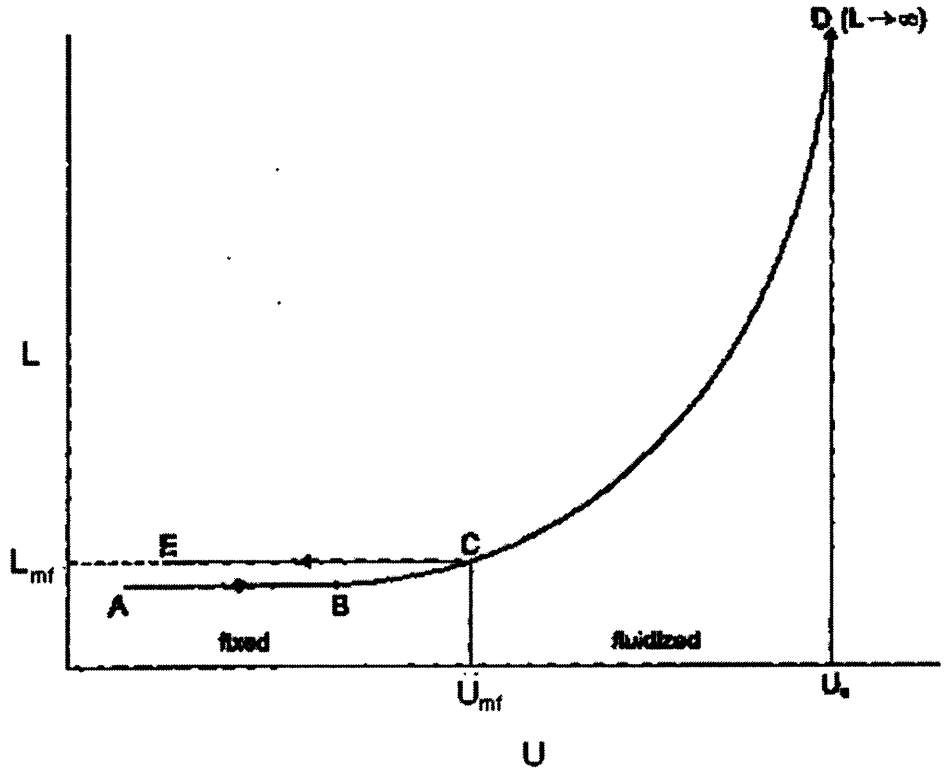

Figure 1.3 Bed height versus superficial velocity of liquid (Wen et al. 1966).

Richardson and Zaki (1954) developed a correlation indicating that the ratio of the superficial and terminal velocities is an exponential function of the void fraction in the

bed. Since Nanogel® particles are lighter than water; they can be fluidized in the reverse direction compared to the conventional fluidization.

Fan et al. (1982) studied the hydrodynamics of two phase and three phase inverse fluidized beds of polyethylene and polypropylene spherical particles and measured the bed expansion and pressure drop. They proposed two models for inverse fluidized bed expansion. One of them uses the Richardson-Zaki approach and another uses a correlation based on their data for different ranges of the Reynolds number.

Nikov et al. (1991) studied the liquid-solid inverse fluidized bed to determine mass transfer characteristics by finding the mass transfer coefficients as a function of the superficial liquid velocity. An electrochemical method based on the reduction of ferricyanide ions at the surface of a spherical cathode was used to measure the mass transfer coefficients. They also used liquids with different viscosities and effective diffusion coefficient. They found that the effect of superficial velocity was negligible, but increasing the viscosity decreased the mass transfer coefficient. They used 3.6 mm particles (677 kg/m^3) for their experiments. They also found that increasing the density of particles leads to a decrease in mass transfer rate. They used the following relation to describe the mass transfer.

$$Sh = 0.28(GaMvSc)^{0.33} \tag{1.2}$$

where Sh is the Sherwood number, Mv is the density number defined as $[(\rho_l - \rho_s)^2/ \rho_l^2]$, Sc is the Schmidt number and Ga is the Galileo number.

Karamanev et al. (1992) studied the bed expansion characteristics of a liquid-solid inverse fluidized bed of solid particles with diameters from 1.31 to 7.24 mm and densities between 75 and 930 kg/m^3. They found that freely rising spheres do not follow the

standard drag curve and therefore, they proposed a modified drag curve relationship as shown below.

For $12.2<Re_t<130$,

$$\log \mathrm{Re}_t = -1.814 + 1.347 \log N_D - 0.1243(\log N_D)^2 + 0.00634(\log N_D)^3 \quad (1.3)$$

and for $130<Re_t<9 \times 10^4$,

$$\mathrm{Re}_t = \sqrt{\frac{N_D}{0.95}} \quad (1.4)$$

where N_D is Best number defined as [4(Ar/3)].

Ibrahim et al. (1996) studied the gas-liquid-solid inverse fluidized bed of 4- or 6-mm polypropylene particles with a density of about 870 kg/m^3 by finding the gas, liquid and solid holdup through conductivity and static pressure measurements. The conductivity measurements showed that there is a velocity called the uniform fluidization velocity which is the superficial velocity at which the fluidization quality becomes the same throughout the bed. In this study, two independent methods to measure the phase holdup profiles were used. They used a correlation to calculate the liquid holdup from the data obtained by the conductivity method. This equation is

$$\varepsilon_l = (\gamma_r)^{1.27} \quad (1.5)$$

where ε_l is the liquid holdup, γ_r is the ratio of the measured conductance (Γ) at a given condition to the conductance measured with the same electrode in liquid only:

$$\gamma_r = \frac{\Gamma}{\Gamma_0} \quad (1.6)$$

They plotted the solid, liquid and gas holdup profiles. According to the authors the solid and liquid holdup measurements are good techniques to measure the bed height of the

fluidized bed. They suggested that while measuring the bed height in three phase inverse fluidized beds, the measuring technique should be carefully chosen. They found that the bed heights may differ by 30% when two different measurement methods like the conductivity method and the static pressure method are used.

Some hydrodynamic studies of liquid-solid inverse fluidized bed were also done by Bendict et al. (1998). They found that the minimum fluidization velocity (U_{mf}) using different bed heights of the same particles did not change. They also found that U_{mf} decreases with increase in viscosity of the continuous phase in an inverse fluidized bed. In order to increase the viscosity of the fluid they used aqueous solutions of carboxymethyl cellulose (CMC). Moreover, increasing the concentration of CMC in water increased the pressure drop and bed height. Using a multiple regression analysis they found a dimensionless correlation between bed height (H), Reynolds number (Re_p) and Archimedes number (Ar)

$$\frac{H}{H_0} = 2.656\,\mathrm{Re}_p^{1.258}\,Ar^{-0.88} \tag{1.7}$$

They found that this correlation can predict the bed expansion data well within $\pm 20\%$.

Garcia-Calderon et al. (1998) studied the effects of the different biofilm thicknesses, of ground perlite particles, on the hydrodynamics of inverse fluidized bed and also found the bed expansion and terminal velocity which they correlated to the Richardson and Zaki and drag force models. They used synthetic wastewater composed of a mixture of glucose, inorganic salts, and nutrients, as the continuous phase in the inverse fluidized bed of ground perlite particles. They periodically analysed the attached solids (VS), the volatile fatty acid (VFA) and total organic carbon (TOC). It was found that as the biofilm thickness increased, the particle density also increased which lead to a

segregation of particles having different biofilm thickness in the fluidized bed. The particles having larger thickness of biofilm tend to stay at the lowest part of the fluidized bed. The same phenomenon was observed in this work when a layer of oil started accumulating on the aerogel particles, which is described in the later sections of this thesis. Moreover, they also found that the terminal velocity of the perlite particles decrease with an increase in biofilm thickness which is again a reason why the particles will start elutriating out of the bottom of the bed. Also, they found that the biomass accumulation on the particles did not have a significant effect on bed expansion.

The transition from fixed to fully fluidized bed of polyethylene spheres in a gas-liquid-solid inverse fluidized bed was studied by Lee et al. (2000). They studied the gas holdup in gas-liquid flow in the absence of solid particles showing that the gas holdup increased with increasing gas velocity. They also plotted the experimental pressure gradient against the superficial velocity of the water with 5.8 mm particles (density in the range 910 – 946 kg/m^3) in a gas-liquid-solid inverse fluidized bed. The frictional pressure drop in the three phase inverse fluidization follows a hysteresis showing different regimes from fixed-bed to partially fluidized bed and later to fully fluidized bed on increasing the liquid velocity at a constant gas velocity. Figure 1.4 shows the above mentioned hysteresis. The pressure drop rises steeply from points O to A which indicates that it is a packed bed where the water simply passes through the voidage of the bed until the pressure drop reaches a maximum value at point A. Half or less of the bed is stationary on or after point A. When the liquid velocity is further increased the pressure drop decreases slightly until the point B and then the bed becomes fully fluidized as indicated by a constant pressure drop from point B to C. But if the liquid velocity is allowed to

decrease then the pressure drop does not follow the path when the velocity was increased. Instead, the pressure drop remains low and follows the path traced by the points C, B, A' and O.

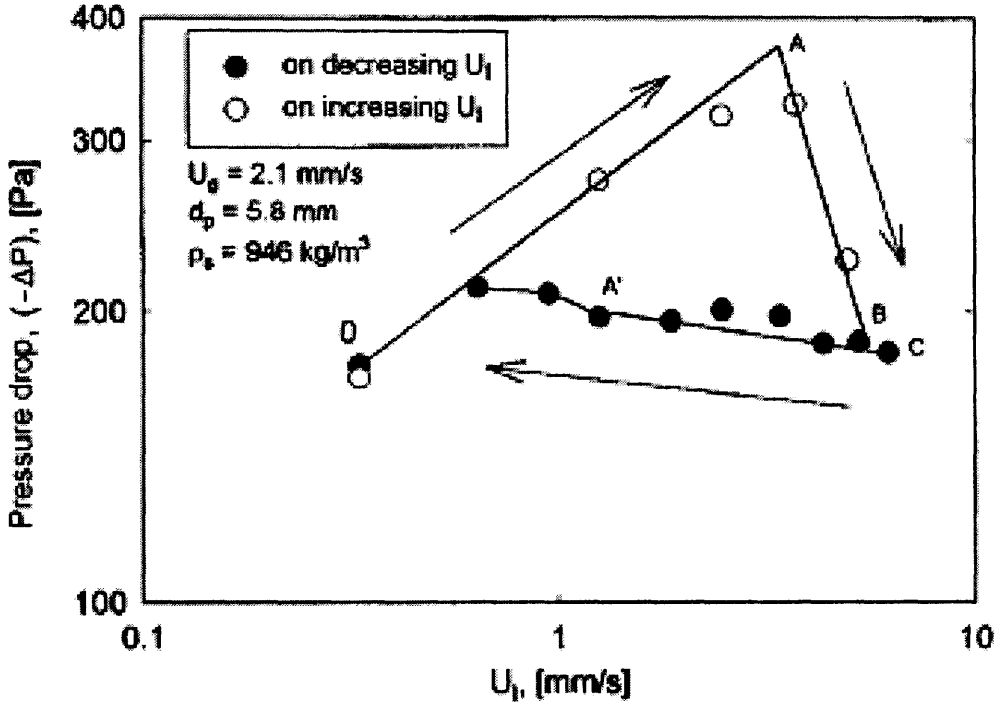

Figure 1.4 Pressure drop for three-phase inverse fixed and fluidized beds of polyethylene beads (Lee et al. 2000).

They also found that increasing the gas velocity will decrease the minimum fluidization velocity of the particles. On increasing the gas velocity, the gas holdup increased, the liquid holdup decreased and the solids holdup remained constant.

Heat transfer and other hydrodynamic characteristics in two- and three- phase inverse fluidized beds of polyethylene and polypropylene particles were studied by Cho et al. (2002). They installed a heater rod at the center of the column and used iron-constantan thermocouples to measure the temperatures at the heater surface and the fluidized bed. They used semi-conductor type pressure sensors to measure static pressure

along the axial direction of the bed. It was found that as the liquid velocity increased, the heat transfer coefficient increased and then started reducing. This was because as the liquid velocity increased there was an increase in the movement of solid particles in the fluidized bed which increased the heat transfer coefficient; but if the liquid velocity is too high, the solids holdup could decrease which could lead to less turbulence and therefore a lower heat transfer coefficient. They also found that by using particles of two different densities that the heat transfer coefficient increases by increasing the density of particles. In the three phase inverse fluidized bed, the heat transfer coefficient shows a maximum which indicates that a further increase in liquid velocity may lead to elutriation of particles leading to reduction in solids holdup, thereby decreasing the heat transfer. They also predicted the Nusselt number and compared it with the experimental results and found a good fit of the data.

Renganathan et al. (2003) developed some general equations for predicting the minimum fluidization velocity for various flow regimes in liquid-solid and gas-liquid-solid inverse fluidized beds (IFBs) based on their experimental data and from the data available in the literature. Their empirical equations are given in Table 1.1. They studied particle diameters ranging from 0.18 mm to 12.6 mm (with densities ranging from 250 to 693 kg/m^3) for the two-phase IFB and 6.1 to 12.1 mm (with densities of 860 and 835 kg/m^3) for the three-phase IFB. They also found that the classical Wen and Yu equation for calculating minimum fluidization velocity is also valid for inverse fluidized beds. Moreover, they checked the validity of the Gas Perturbed Liquid Model (GPLM) The GPLM assumes that full support of the solid phase is provided by the liquid phase and the space occupied is being perturbed by the gas phase. This model did not seem to fit the

experimental data for the three phase IFB. Therefore, they modified the GPLM as shown in Table 1.1.

Table 1.1 Equations Classified According to the Range of Archimedes Number

Range $Ar \times 10^4$	Imperical equation	RMS Error %	Modified GPLM	RMS Error %
Low 1.47 – 8.47	$Re_{mf} = Re_{mf0} - 0.176Ar^{0.434}Re_g^{0.669}$	29	$Re_{mf} = \sqrt{33.7^2 + 0.0408Ar\left(1 - 21.2Ar^{-0.292}Re_g^{0.549}\right)} - 33.7$	30
Medium 9.97 – 151	$Re_{mf} = Re_{mf0} - 0.0692Ar^{0.438}Re_g^{0.839}$	14	$Re_{mf} = \sqrt{33.7^2 + 0.0408Ar\left(1 - 1.181Ar^{-0.097}Re_g^{0.586}\right)} - 33.7$	16
High 294 – 1472	$Re_{mf} = Re_{mf0} - 0.00185Ar^{0.578}Re_g^{0.882}$	11	$Re_{mf} = \sqrt{33.7^2 + 0.0408Ar\left(1 - 0.152Ar^{-0.0111}Re_g^{0.555}\right)} - 33.7$	13
Low 1.47 – 8.47	$Re_{gmf0} = \left(\frac{Re_{mf0}}{0.176Ar^{0.434}}\right)^{1/0.669}$		$Re_{gmf0} = \left(\frac{1}{21.2Ar^{-0.292}}\right)^{1/0.549}$	
Medium 9.97 – 151	$Re_{gmf0} = \left(\frac{Re_{mf0}}{0.0692Ar^{0.438}}\right)^{1/0.839}$	28	$Re_{gmf0} = \left(\frac{1}{1.181Ar^{-0.097}}\right)^{1/0.586}$	23
High 294 – 1472	$Re_{gmf0} = \left(\frac{Re_{mf0}}{0.00185Ar^{0.578}}\right)^{1/0.882}$		$Re_{gmf0} = \left(\frac{1}{1.152Ar^{-0.0111}}\right)^{1/0.555}$	

Source: Renganathan et al. (2003)

Renganathan et al. (2004) tried to simulate the pressure drop, bed voidage and minimum fluidization velocity of an inverse fluidized bed under steady-state conditions and unsteady-state bed expansion/contraction by a Monte Carlo (MC) technique. They used 1000 particles as a basis for their simulation and compared the results against the experimental values of the hydrodynamic parameters. They found that the simulated results of pressure drop and bed expansions were in good agreement with the experimental data for larger particles. The error between MC and the Wen and Yu equation for simulating the minimum fluidization velocity was 19%, and the error

between MC and the experimental minimum fluidization velocity was 25%. The equation used for the simulated pressure drop was:

$$\Delta P = \frac{NF_D}{A} \tag{1.8}$$

where A is the cross section area of the simulation space, N is the number of particles in the simulation space, F_D is the drag force given by

$$F_D = V_P \left[\frac{150\mu_l u_l (1-\varepsilon_{loc})}{d_p^2 \varepsilon_{loc}^3} + \frac{1.75\rho_l u_l^2}{d_p \varepsilon_{loc}^3} \right] \tag{1.9}$$

when the pressure drop is to be calculated for the packed bed regime (from Ergun equation) and drag force for the fluidized bed regime (from Khan and Richardson (1954) equation) is given by

$$F_D = C_D \varepsilon_{loc}^{-2n} \frac{\rho_l u_l^2}{2} \frac{\pi d_p^2}{4} \tag{1.10}$$

where C_D (drag coefficient), is given by:

$$C_D = \frac{\frac{4}{3} Ar}{\mathrm{Re}_t^2} \tag{1.11}$$

The quality of fluidization elucidated by the local voidage fluctuations was also studied by Renganathan et al. (2005). In order to find the local void fraction of the bed, they again used the conductance method. They predicted the bed expansion using the Richardson-Zaki equation and the Drift Flux model (Wallis, 1969). The Drift Flux model assumes that the interaction between the solid and liquid phases of an IFB can be described by a relation between the drift velocity as a function of phase holdups. Renganathan et al. (2005) were able to develop a correlation based on the correlation of Turton and Clark's (1987) approach for the terminal velocity and compared the

calculated results against the experimental results. They found that this equation was able to fit the experimental terminal velocity with an RMS error of 12% which is shown in Figure 1.5. The equation proposed by them is given below:

$$u* = \left[\left(\frac{18}{d*^2} \right)^{0.776} + \left(\frac{1.713}{4d*^{0.5}} \right)^{0.776} \right]^{-1/0.776} \tag{1.12}$$

where $u*$ is given by

$$u* = U_i(\rho_l^2 / (g\mu_l(\rho_l - \rho_p)))^{1/3} \tag{1.13}$$

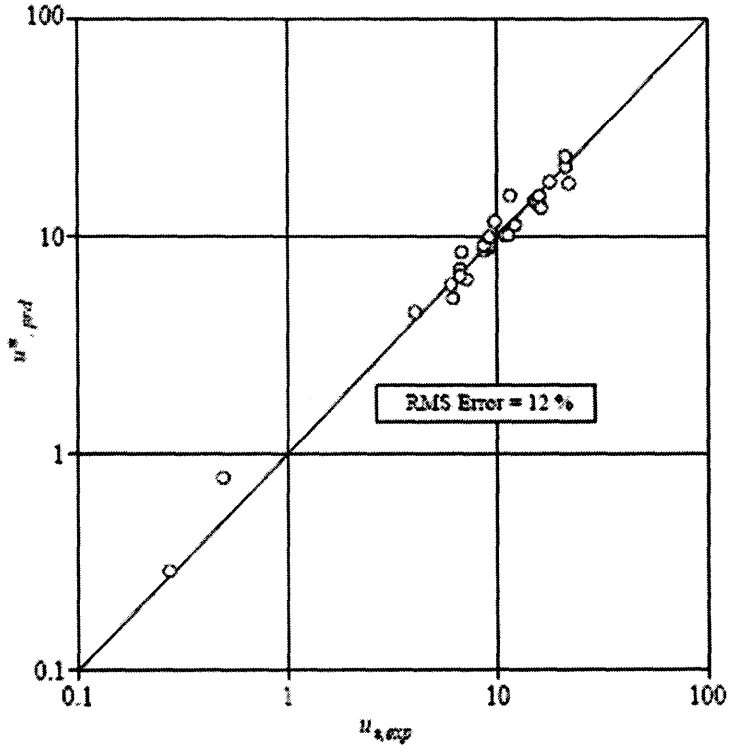

Figure 1.5 Comparison of experimental and predicted terminal velocities (Renganathan et al. 2005).

and $d*$ is given by

$$d* = d_p((\rho_l - \rho_p)\rho_l g / \mu_l^2)^{1/3} \tag{1.14}$$

In the Figure $u_{*,\exp}$ is found by extrapolating the experimental bed expansion data to $\varepsilon = 1$.

Renganathan et al. (2004) were also involved in studying the liquid phase residence time distribution (RTD) for a liquid-solid inverse fluidized bed. For this purpose, they determined the RTD of the system, the residence time, the Peclet number and the axial dispersion coefficient by using a pulse tracer technique. For the online measurement of the tracer, injected at the top of the column, they used the conductivity method. The tracer used was a NaCl solution (*5 N*) and the conductivity was measured by placing several SS 314 electrodes at the inside surface of the column which was connected to a computer. The concentration of tracer was measured in terms of voltage which was converted to salt concentration using a calibration equation based on separate experiments. They tried to find the effect of liquid velocity, static bed height and particle characteristics on the liquid phase axial dispersion coefficient. They found that the coefficient increases with increase in liquid velocity, remains stable with increase in static bed height, and increases with increase in Archimedes number. An increase in liquid velocity or Archimedes number will tend to create more flow of liquid meaning more turbulence in the fluidized bed resulting in better mixing. They also developed a correlation based on their experimental data to predict the liquid phase axial dispersion coefficient which is shown in Equation (1.15)

$$D_l(cm^2/s) = 1.48\times10^{-4} Ar^{0.66}\left(\frac{\mathrm{Re}}{\mathrm{Re}_{mf}}\right)^{1.73} \qquad (1.15)$$

In this equation the Re_{mf} is determined from the Wen and Yu equation. This correlation is valid for $17.6<Ar<1.47 \times 10^7$ and $0.036<Re<1267$.

Based on all of the above mentioned research work using inverse fluidized beds by different researchers, calculations for finding some of the parameters such as the minimum fluidization velocity, void fraction, particle terminal velocity and granule size were done in this work. For example, the Richardson-Zaki model was used to find the terminal velocity and granule size. Moreover, the Wen and Yu equation and the Frantz correlation were used to find the theoretical minimum fluidization velocities which were then compared with the respective experimental values.

1.6 Current Oil Removal Techniques

Some of the techniques that are currently used to remove oil from water are gravity separation, centrifugal separation, membrane ultrafiltration, air flotation, biological treatment or chemical treatment, and deep bed adsorption.

In order to develop a cost effective treatment plant, the oily water is treated in several steps which include primary treatment, secondary treatment and tertiary treatment. These steps will also include the removal of other contaminants present in water like suspended solids, organic and inorganic chemicals, heavy metals, etc. The primary treatment may include the use of gravity separators and centrifugal separators. The secondary treatment may include the use of Induced Air Flotation devices, and biological treatment or chemical treatment. Tertiary treatment may include the use of ultrafiltration, microfiltration and carbon adsorption equipment. A brief summary of several methods employed industrially for the treatment of oily water is given in Table 1.2.

Table 1.2 Overview of Existing Water Treatment Processes for Oil Removal

Unit Process	Description	Advantages	Limitations
API Separator	A simple gravity separator whereby the oil floats on water and is mechanically collected.	Free oil is easily removed giving removal efficiencies from 50 – 90%.	Soluble oil cannot be removed. Free oil content downstream can range from 15-100 ppm.
Induced Gas Flotation	Air is bubbled through the oil-water mixture which produces foam. The oil attached to the foam is then skimmed from the top.	Removal efficiencies can reach to 93% and can be enhanced even more by adding foaming agents.	Not capable to remove soluble contents.
Hydroclone	A centripetal field generated by high flow of fluid entering a cylindrical cyclone separates the heavier components like water from the lighter components like oil.	Better than API separator and Induced Gas Flotation in terms of oil removal efficiency and it also occupies comparatively less space.	Highly soluble oil components are not removed. Operating cost will be high due to high pumping cost.
Deep Bed Filter	A layer of sand or other granular media in a cylindrical tank removes oil from water.	The size of oil droplets are removed depending upon the size of the granules in the deep bed filter.	Soluble organics are not removed. Cannot handle influent oil concentrations higher than 100ppm.
Ultrafiltration and microfiltration	A membrane capable of filtering solutes as small as 1000 daltons is used.	Very efficient in removing oil (about 85 – 99% of total oil). Compact design uses less space	Fouling of membrane is a problem leading to reduction in permeate flux or high pumping costs.

Source: Hayes et al. (2004).

Water contaminated with oil can be classified according to the size of the droplets present in the water (Manning et al., 1983). If the oil droplets have a size below 20 μm, it is called an emulsified oil mixture and if the size of oil droplets is between 20 and 150 μm it is called a dispersed oil mixture and if the oil droplets have a size greater than 150 μm then it is called free oil according to the Manual on Disposal of Refining Wastes (1969). Moreover, if the oil in the oil-water mixture is not in the form of droplets then it is said to be soluble. Figure 1.6 summarizes the classification of oil-water mixtures according to oil droplet size and the corresponding removal methods. Since the micro-

organisms cannot withstand high concentrations of oil in water the biological treatment of oil-water mixtures is limited to low concentrations of oil in water.

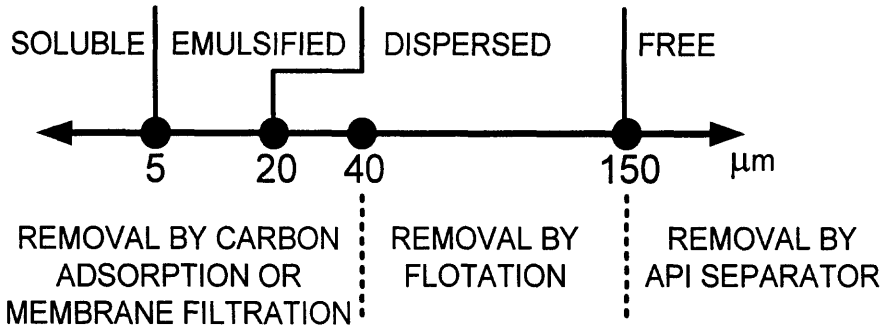

Figure 1.6 Classification of oil-water mixtures according to droplet size and corresponding removal methods.

Any device or piece of equipment that utilizes the difference in density of oil and water to remove oil from water is called an Oil-Water Separator (OWS) which is shown in Figure 1.7. While studying the oil-water separation theory, the first step is to look into the Stokes' Law which is expressed as:

$$v = h/t = (D_p^2 g(\rho - \rho^1))/18\vartheta \tag{1.16}$$

where v is the terminal velocity, ρ is the density of water and ρ^1 is the density of oil and ϑ is the viscosity of the continuous phase. Since the droplet diameter is squared, it has a very strong effect on the efficiency of separation, so it is important to increase the droplet size. This is done by using coalescing devices like oleophilic meshes, porous media, coalescence plates, etc. It is important to note that most of the oil-water separators work on the above principle taking advantage of one or more parameter like the droplet diameter, density difference between oil and water and the viscosity of oil.

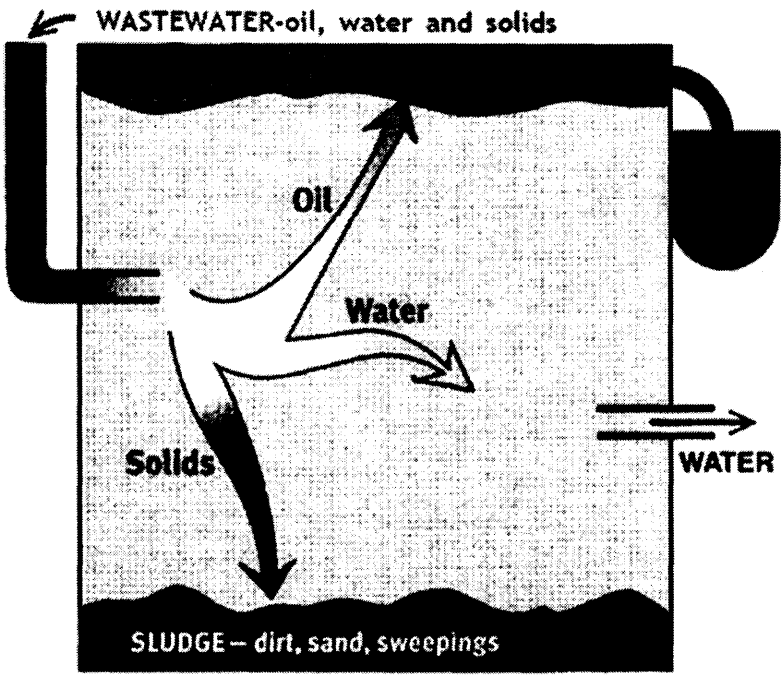

Figure 1.7 A simple Oil Water Separator (EPA US., 1999).

There are different types of OWS using different mechanisms. The American Petroleum Institute (API) separator shown in Figure 1.8 is used to remove free oil from waste water. These separators basically depend on the residence time of the oil droplets in order to coalesce and form an oil layer which can be skimmed off; therefore they are also called oil skimmers. The skimming process can be done by using a belt skimmer or an overflow weir.

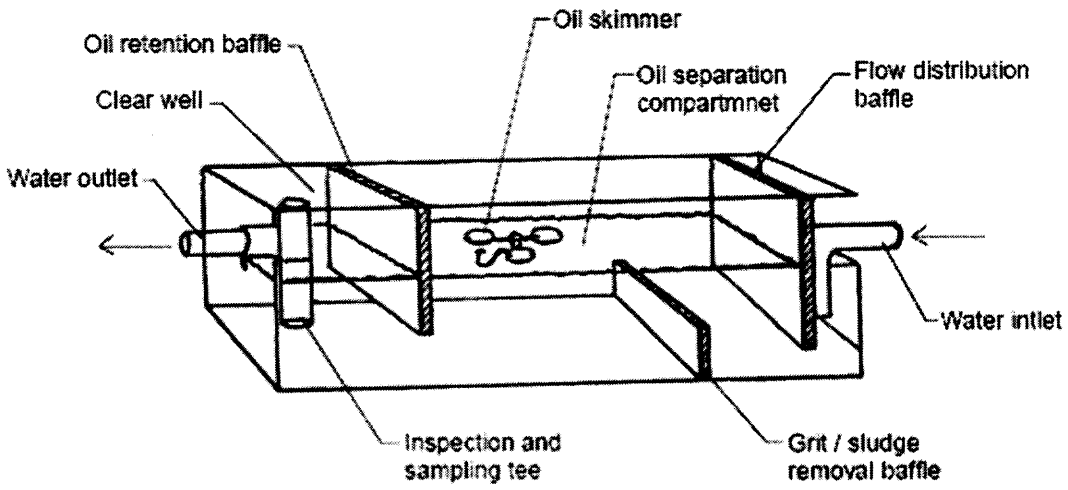

Figure 1.8 The American Petroleum Institute (API) type separator perspective view (National Conference on Urban Runoff Management., 1993).

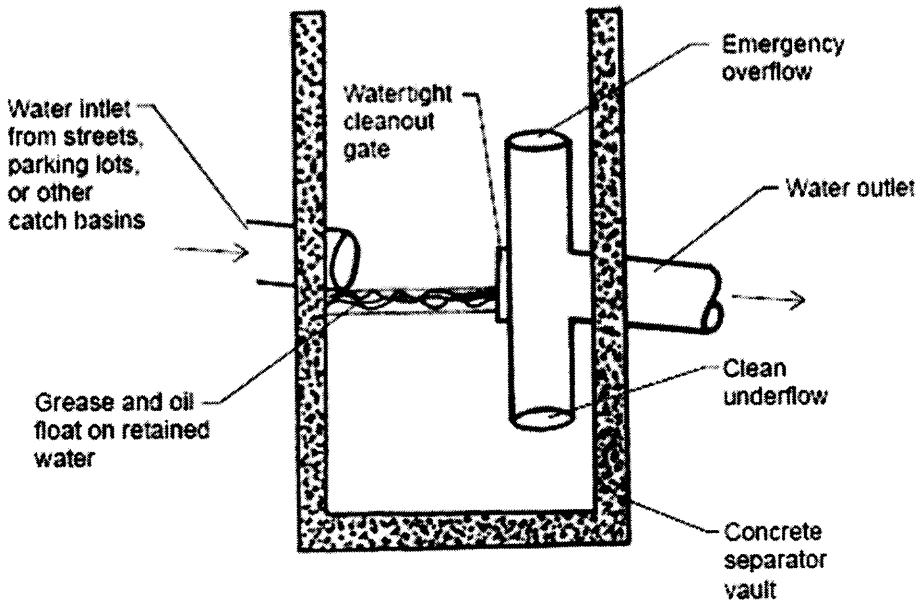

Figure 1.9 The Spill Control type separator section view (National Conference on Urban Runoff Management., 1993).

A Spill Control type separator shown in Figure 1.9 is used for removal of oil and grease from water coming from streets runoff, parking lots, and other catch basins. For

the secondary treatment of oily water, Induced Gas Flotation (IGF) and Dissolved Gas Flotation (DGF) units are used. They involve the introduction of fine gas bubbles that attach to the oil and fine solids and float them to the surface where they are removed. Flotation units can remove up to 95% of free oil. They are mostly used as a separation step downstream of gravity separation to either meet discharge limits for oil and grease or save filtration from extremely short run lengths. They still have a limitation that the inlet oil content should not exceed 300 mg/L as the outlet oil removal suffers above this limit. The flotation systems are good for removal of dispersed oil, but their operating cost is high because of the need to add coagulants and pH regulators in addition to injecting air into the system.

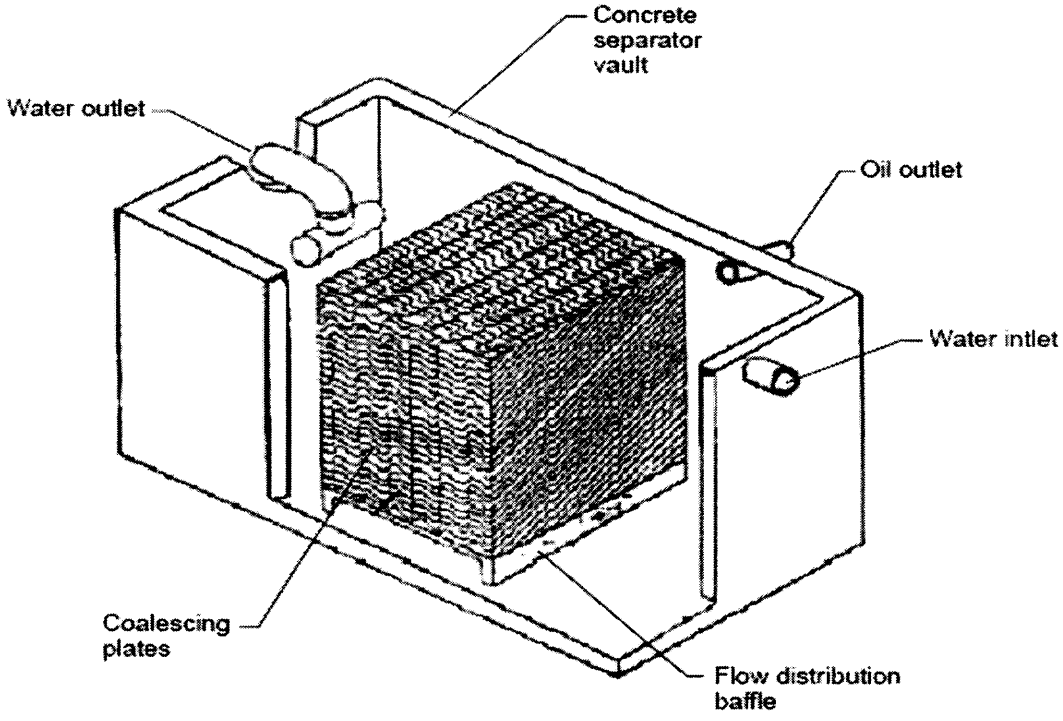

Figure 1.10 Coalescing Plate type separator perspective view (National Conference on Urban Runoff Management., 1993).

A Coalescing Plate Separator shown in Figure 1.10 uses a coalescing media made of corrugated Polyvinyl Chloride (PVC) which attracts the smaller oil droplets to its

surface where they coalesce to form a larger droplet which quickly rises to the top according to Stokes' Law and then gets separated.

Another way of coalescing the oil droplets is by chemical injection of flocculants or coagulants and mechanical agitation. Chemical injection presents a disadvantage in that it may pollute the water and create a need to be removed later. The mechanical agitation requires more power which is again a disadvantage. A good description regarding gravity driven separation is given by Gaaseidnes et al. (1999) which includes oil-water separators such as gravity separators, coalescing plate separators, inverted cone, oil skimmers, and centrifugal separators.

The above mentioned OWS are able to remove free oil and dispersed oil but are poor in efficiency to remove dissolved or emulsified oils. Another well known process used as an alternative method to gravity separators is centrifugal separators like hydroclones. A centrifugal force of a magnitude of 10000 times that of gravity is applied on the fluids whereby the water moves to the wall of the conical apparatus and the oil migrates to the center at the core of the hydroclone. It requires a high pressure flow which can generate the high velocity needed for the centrifugal force. This is a limitation of this system. Similar equipment is a centrifuge which applies mechanical moving parts for the oil/water separation instead of high pressure flow of water. But this equipment has a disadvantage of high operating costs. Deep bed adsorption filtration and membrane filtration (Goldsmith, 1973) are techniques which are being used to remove dissolved and emulsified oil from water. Although these techniques are very efficient in removing oil their capacity is limited; moreover, membrane filtration requires high pressures and good quality feed which increases its operating and capital costs.

Ultratfiltration can isolate emulsified oil droplets from water. Generally it uses a semipermeable polymer membrane with a constant pore size (0.0015 to 0.20 microns) which can eliminate all the contaminants greater than the specified pore size of the membrane (Goldsmith et al., 1973). With this system, it is possible to obtain an oil-free solution and an oil-rich concentrate. Figure 1.11 shows the working of an ultrafiltration membrane where the contaminated liquid enters at high pressure and the purified liquid called the permeate passes through the pores of the membrane leaving behind a concentrate consisting of all the contaminants.

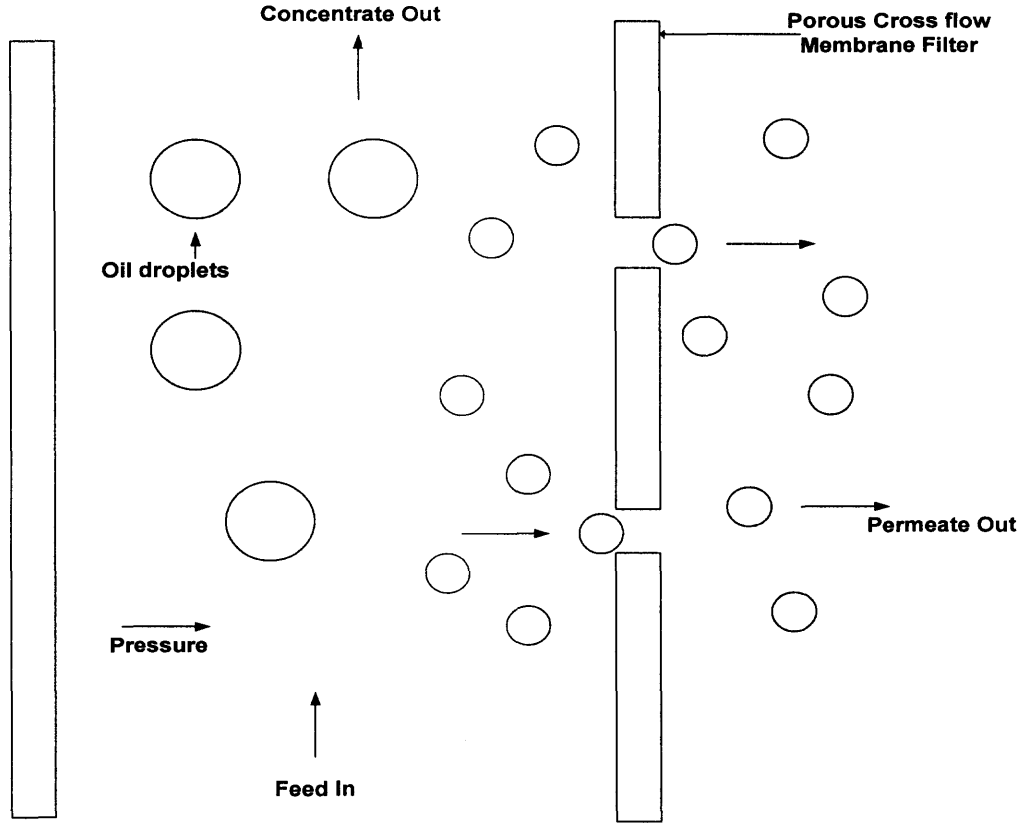

Figure 1.11 The working of an Ultrafiltration membrane.

Filtration techniques such as ultrafiltration require high energy consumption and they have limited capacity owing to their specific permeability which determines the resistance of the media for the contaminated water flowing through it. The permeability is usually checked by looking at the pressure drop across the filter, which increases as the permeability decreases due to saturation of the media with the contaminants. In order to maintain a reasonable energy consumption, the water flowing through the filter has to be reduced or else the pumping costs will increase. But if the throughput has to be kept constant then the pumping power has to be increased leading to high energy consumption. Chemical treatment is another method which uses a salt or a polymer with an acid to destabilize the emulsion and subsequently separate oil from water by using a mechanical device like an oil-skimmer (Furrow, 2005).

Another approach to filter contaminants from water is the use of a porous medium.

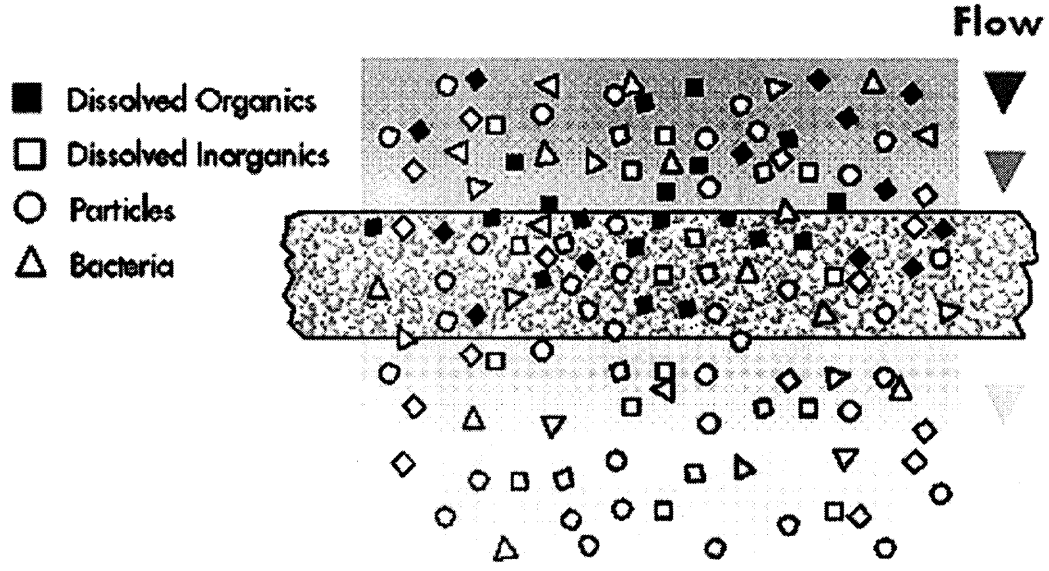

Figure 1.12 A granular bed filter with Granular Activated Carbon as filter media.

A porous medium is a solid containing many holes and tortuous passages. Figure 1.12 shows a schematic of a granular bed filter using activated carbon. A granular bed filter uses several mechanisms to capture oil from water depending upon the flow pattern and the size of the oil droplets.. The granular bed or deep bed may be composed of either a monosized filter media or it may be composed of several layers of different sized filter particles. Cambiella et al. (2006) studied the performance of sawdust as a filter media for the treatment of an oil-water mixture. They passed an influent oil concentration of 24000 mg/L through a deep bed filter consisting of a Eucalyptus saw dust (density of 782 kg/m^3 and porosity of 66.5%) layer. They also used some calcium sulphate in the sawdust bed in order to neutralize the charge on the oil droplets for better adsorption on the sawdust surface. They measured the pressure drop, oil content and Chemical Oxygen Demand (COD) values in the effluent by varying the operating condition such as flow rates, amount of coagulant salt, bed height and temperature. The oil concentrations were measured by IR spectroscopy, using a Horiba OCMA 310 oil content analyzer. Although it was found that 95% of COD was removed, the higher pressure drop across the packed bed filter would have resulted in a lower flux of purified water.

Mysore et al. (2005) studied the efficacy of alumina-silicate resembling mica called vermiculite (bulk density of 70 kg/m^3 and porosity of 75%) to treat oily waters. Their experimental procedure mostly involved column studies in a 30 mm diameter and 400 mm long acrylic pipe with a 300 mm depth of vermiculite. The flow rate of oil-in water emulsions was 3 mL/min and the experiment was run for 8 hours. They tried four different types of oil and found that the oil removal efficiencies were between 43 to 93%. The performance of different filter media with different type of oil (SMO, KUT45, RE) is

shown in Table 1.3. They also found that the kinetic data satisfied the Lagergren (1898) and Ho (1999) model, while the equilibrium studies showed that the Langmuir (1916) isotherm fitted the oil removal by vermiculite particles. They also tried to fit the experimental data into two kinetic models. The first model was the kinetic equation derived by Thomas which is

$$\frac{C}{C_0} = \frac{1}{1 + e^{k/Q(q_0 m - C_0 V)}} \tag{1.17}$$

The second model was as suggested by Weber and Morris (1963) for adsorption where the uptake of the solute varies for reactions controlled by intraparticle diffusion.

$$\frac{X}{M} = St^{1/2} \tag{1.18}$$

Table 1.3 Comparison of Oil removal Efficiencies of Vermiculite and Other Sorbents

Emulsion/Sorbents	Initial oil concentration (mg/l)	Final oil concentration (mg/l)	Percentage removal
SMO			
0.5g of bentonite	502	11.0	97.8
0.5g of powdered organo clay	235.5	11.2	95.3
5.0g of organo clay/anthracite	236.6	49.8	79.0
1.5g of expanded vermiculite	218	45	79.0
1.5g of hydrophobized vermiculite	218	65	56.0
KUT45			
0.5g of bentonite	305	12.4	95.9
0.5g of powdered organo clay	381	3.8	99.0
5.0g of organo clay/anthracite	330	70.8	78.6
1.5g of expanded vermiculite	170	18.0	89.4
1.5g of hydrophobized vermiculite	170	90	49.0
RE			
0.5g of bentonite	5.2	0.7	95.3
0.5g of powdered organo clay	5.2	2.4	53.9
5.0g of organo clay/anthracite	5.2	0.1	98.1
1.5g of expanded vermiculite	11.5	4.9	57.0
1.5g of hydrophobized vermiculite	11.5	6.5	43.0

Source: Mysore et al. (2005).

Ribeiro et al. (2003) studied the effectiveness of a hydrophobic aquatic plant, a *Salvinia* sp., as an oil filter for oil/water emulsions. They also compared its performance with processed peat (Peat Sorb). For the *Salvinia* sp., the amount of oil retained was 1.33 g oil/g biomass and for the Peat Sorb the amount of oil retained was 0.26 g oil/g biomass. These results show a better removal capacity of *Salvinia* sp. The superiority of the aquatic plant over the Peat Sorb is because of its hydrophobicity and the hair like projections of the surface of the biomass.

Hrubesh et al. (2004) have compared the adsorption capacity of hydrophobic silica aerogel against granulated activated carbon in removing certain organic solvents from water. Their results are shown in Table 1.4.

Table 1.4 Comparison of Adsorption Capacities of Hydrophobic Silica Aerogel and Granulated Activated Carbon

	Adsorption capacity (gm/gm)	
Solvent	**Hydrophobic Silica Aerogel**	**Granulated Activated Carbon**
Toluene	0.833	0.026
Cyclohexane	0.458	0.011
Trichloroethylene	11.89	0.091
Ethanol	1.94	0.028

Source: Hrubesh et al. (2004).

Pasila et al. (2004) studied the possibility of using natural materials like reed canary grass, flax and hemp fibre as oil adsorbing filter materials. These materials were first freeze treated, dried, milled and then fragemented before being used as filter media. Experiments were performed by making an oil water mixture by adding 80 ml of oil in

200 ml of de-ionized water and passing this mixture through 10 or 20 g of adsorption filters. The hemp fibre and reed canary grass fragments adsorbed 2-4 g of oil per gram of adsorption material.

Some other filter media have also been studied to investigate the possibility and efficacy of these filters to remove oil from water. Other examples of naturally occurring filter medium which can be used in a packed bed filter include activated carbon, peat (Mathavan et al., 1989), bentonite, and organoclay. An EPA report (2006) discusses about the use of different commercially available sorbent materials to remove oil from storm waters (Stenstrom et al., 1998). The report is related to finding the oil removal efficiencies of sorbent materials (Nanofiber, OARS®, Rubberizer®, Sponge Rok, and Xsorb) in a Continuous Deflection Separation (CDS) device. Alsaigh et al. (1999) studied the efficiency of four different Best Management Practices (BMPs) that use sorbent materials (Hydrocartridge®, StreamGuard®, Gullywasher®, Grate Inlet Skimmer Box).

Figure 1.13 is an example flow sheet of a filtration plant devised to filter influent oil and grease concentration of 59 mg/l along with dissolved solids and Total Organic Carbon. Since polluted water has a number of different contaminants, different techniques have to be applied in series to remove these contaminants. The inverse fluidization column described in this thesis can be fitted to replace the Walnut Shell filter shown in Figure 1.13.

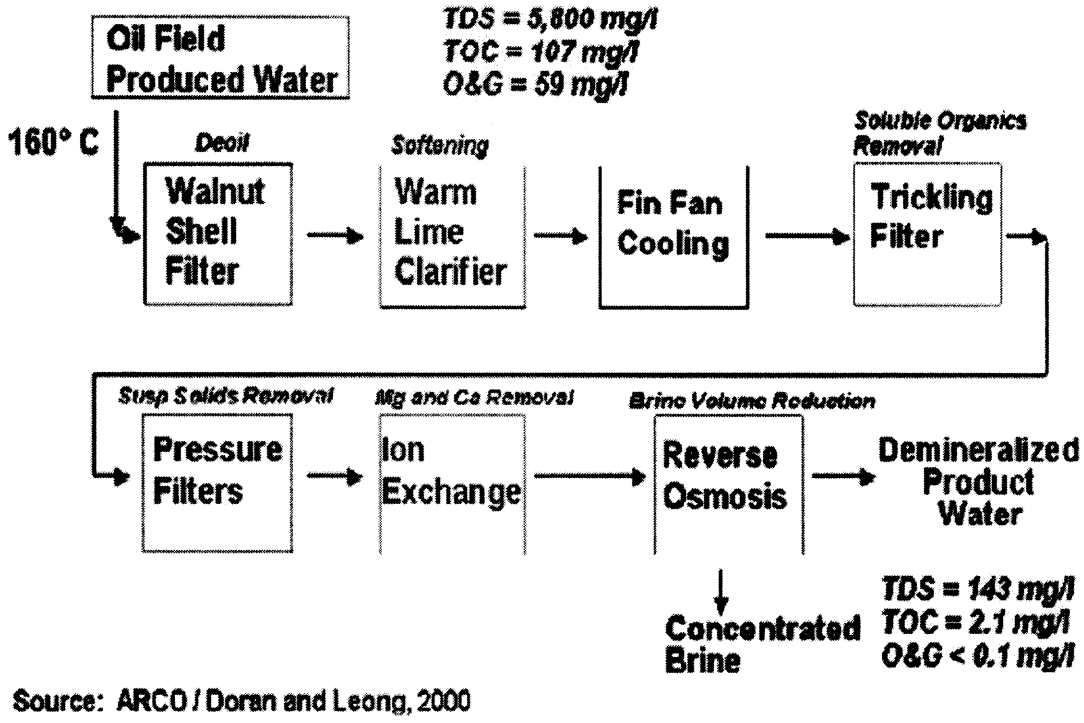

Figure 1.13 A typical example flow sheet of a filtration plant.

Current systems also involve an inverse fluidized bed system for waste water treatment, which is called the inverse fluidized bed bio-reactor. These reactors employ a thin layer of micro-organisms on the solid particles which are then inversely fluidized in a column. The waste water is then contacted with the inversely fluidized particles so that the micro-organisms present on their surface could digest the hydrocarbon waste. Although this technique is efficient in removing hydrocarbons from water, it has one major disadvantage. Since micro-organisms grow exponentially, there is a problem of contamination of water released from the inverse fluidized bed bio-reactor. Therefore additional arrangements are needed to remove these micro-organisms, which can incur more operational cost to the system. But, if an inverse fluidized bed system is used to

remove oil from water without using micro-organisms, the problem of contamination might be prevented. Therefore, the inverse fluidized bed system presented in this thesis could be a possible solution for the removal of oil from water.

CHAPTER 2

INVERSE FLUIDIZATION OF NANOGEL

2.1 Introduction

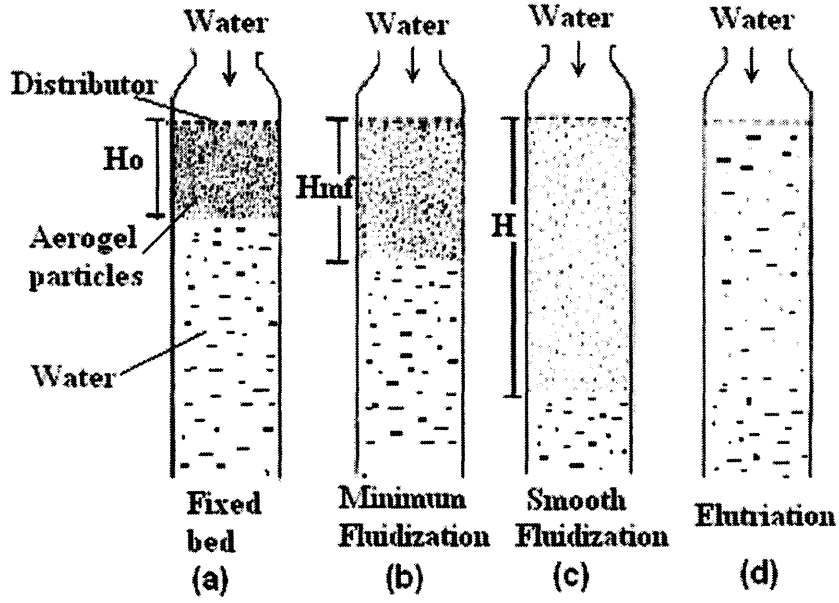

Figure 2.1 Different stages of inverse fluidization by increasing the fluid velocity.

In conventional solid-liquid fluidization when a liquid flow is introduced through the bottom of a bed of solid particles, it will move upwards through the bed via the empty spaces between the particles. At low fluid velocities, hydrodynamic drag on each particle is low, and thus the bed remains in a fixed state. Increasing the velocity, the drag forces plus the buoyancy due to the liquid will begin to counteract the gravitational forces, causing the bed to expand in volume as the particles move away from each other. Further increasing the velocity, it will reach a critical value at which the upward drag forces plus the buoyancy forces will exactly equal the downward gravitational forces, causing the particles to become suspended within the fluid. At this critical value, the bed is said to be

fluidized and will exhibit fluid-like behavior. By further increasing liquid velocity, the bulk density of the bed will continue to decrease, and its fluidization becomes more violent, until the particles no longer form a bed and are "conveyed" by the liquid flow.

In inverse fluidization the direction of the flow of liquid is reversed and the solid particles have a lower bulk density compared to the liquid, which means that the solid particles tend to float on the liquid and hence stay at the top of the fluidized bed column. So, in order to fluidize the solid particles the liquid should enter from the top of the column flowing downwards. In this case, the hydrodynamic drag force has to counteract the buoyancy force due to the liquid and gravity force due to the weight of the particles. Figure 2.1 shows different stages of inverse fluidization when the velocity of the liquid is gradually increased. Figure 2.1(a) indicates that the velocity of liquid is not enough to fluidize the bed of solid particles with a bed height of H_0. When the liquid velocity is increased to Umf, the bed of particles start expanding which is shown in Figure 2.1(b) with a bed height of H_{mf}. Further increasing the velocity leads to a large bed expansion indicated by H and smooth fluidization as shown in Figure 2.1(c). Increasing the velocity even further may lead to conveying of the solids (elutriation or entrainment) to the exit of the column as shown in Figure 2.1(d).

2.2 Experimental Setup and Procedure

Figure 2.2 shows a schematic diagram of the experimental setup employed for all the experiments on inverse fluidization of aerogel by using water as a continuous phase. The setup consists of a fluidization column, a pressure gauge, a differential pressure

transmitter with a display, two flowmeters, a static mixer, and a metering pump, along with the respective valves and piping.

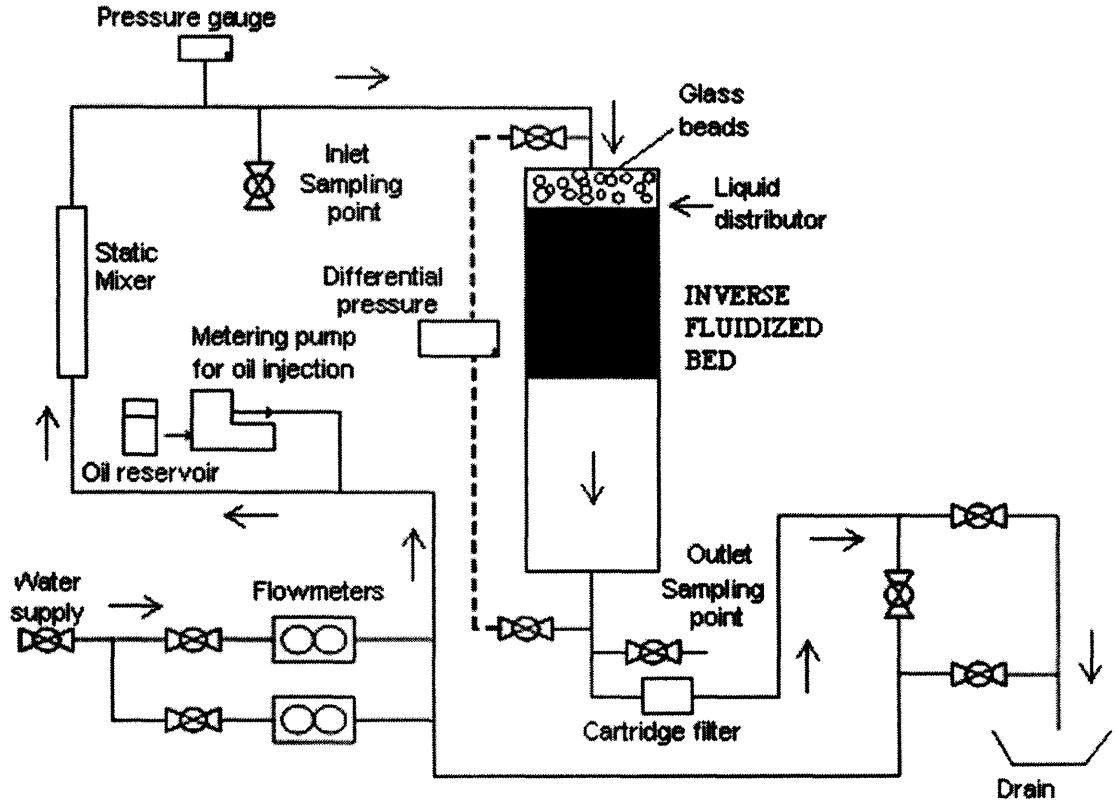

Figure 2.2 Schematic diagram of the inverse fluidization experimental setup.

The valves were adjusted to get a constant flow rate of water which entered at the top of the column through a distributor and flowed downwards. The liquid distributor was made up of a packed bed of glass beads of 3 to 4 mm in size and with a depth of 1.5 inches. As expected, the packed bed of aerogel granules at the top of the column remained as a packed bed until the flow is increased to such a point that they are fluidized in the downward direction.

The column used for inverse fluidization of aerogel was made of transparent acrylic cylinder having an internal diameter (ID) of 89 mm and an outer diameter (OD) of

101 mm. The length of the column was 0.86 m. The piping and the valves were made of PVC having a diameter of 1 inch. The setup included two calibrated electronic digital flowmeters, one for the range between 0 – 3 GPM and the other for the range between 3 – 50 GPM (GPI series A109), this flowmeters also had digital displays.

A Dwyer (Model 645-1) differential pressure transmitter with a range of 0 – 2 psid (0 – 13.8 KPa) and an accuracy of 0.1% was used to measure the pressure drop across the column through two taps situated before and after the column, respectively. This transmitter was connected to a computer through a RS – 232 port and the pressure drop data was collected using a Meterview® software which took the readings after every 2 second interval. There was another tap located before the column that allowed for the reading of static pressure, which was held constant during the runs, by using a WIKA pressure gauge with a range of 0 – 15 psi (0-103 KPa).

The column was fitted with an adjustable design that helped to remove the column for the purpose of cleaning it. The column also had two PVC caps which were easily removable for loading and unloading of the particles when required. The cap, fitted at the top of the column consisted of a distributor made of a packed bed of glass beads supported by a steel wire mesh. The flow of water entered the top of the column through the distributor and before going to the drain it was filtered by a Keystone Sediment filter (Model 2323N) in order to remove any entrained granules. The hydrodynamic characteristics of the aerogel granules were studied without using any oil in the system. It is to be noted that there was no wire mesh at the bottom of the column to retain the particles, but instead the particles were entrained from the column and retained by the cartridge filter situated after the column. This was done because, it was found during

preliminary experiments that the entrained aerogel granules tend to accumulate over the bottom mesh and increased the pressure drop thereby affecting the readings.

Two types of aerogel granules (Nanogel® from Cabot Corp.) were used as the solid phase in these experiments. Both of the granule types were hydrophobic in nature and one was clear aerogel (TLD) and the other was dark aerogel (OGD). Two different size ranges of the particles were chosen by sieving through U.S Standard Sieves to get cuts of 0.5 to 0.85 mm and 1.7 to 2.3 mm. Another size range of particles chosen was 0.5 to 2.3mm unsieved. The aerogel granules are inherently hydrophobic due to the surface treatment done during the manufacturing process. The aerogel granules are highly porous structures having a pore size of approximately 20 nm and a granule density of about 100 kg/m^3. They have a surface area in the range 600 to 800 m^2/g.

The procedure used to measure the hydrodynamic parameters of the inverse fluidized bed column is as follows. Since the pressure drop taps were located across the column and not across the bed of aerogel granules, the pressure drop across the empty column was measured at different flow rates. The pressure drop across the fluidized bed of particles can be found by subtracting the empty column pressure drop from the total fluidized bed pressure drop. The particles to be fluidized were sieved through U.S Standard Sieves to get granules of 500 to 850 um or 1.7 to 2.3 mm in size and then weighed to get the exact amount of powder used in each experiment. Before starting the experiment, it is very important to sieve the granules properly to get the desired cut and remove the unwanted fines and oversized particles. This will ensure proper calculation of other important parameters mentioned in the later sections. The column was filled with water from the bottom making sure that all the air has been removed by a vent at a high

point. After measuring the static bed height and making sure that there were no air bubbles in the inlet and outlet lines of the differential pressure transmitter, the experiment was started by slowly increasing the flow of water and recording the hydrodynamic parameters, once the bed is stable. It is important to note that the flow of water is in the direction from top to bottom of the column and the bed expansion is also from top to bottom. The bed height and pressure drop were measured until the bed expanded to the bottom of the column.

Sieving the granules is an important step. Since the granules are very porous and fragile, vigorous sieving by a sieving machine for a long time could break down the granules leading to formation of fines much smaller than the original granules. These fines may later lead to erroneous pressure drop readings. Moreover, they may also get entrained by the flow of water and clog the cartridge filter quicker than expected. It is also important to remove air bubbles from the column and also from the inlet and outlet line of the differential pressure transmitter. These air bubbles interfere with the pressure drop readings of the inverse fluidized bed. When the pressure drop of inverse fluidized bed is measured, it is important also to check whether there is any elutriation of the particles. Elutriation of particles may reduce the fluidized bed height as well as the mass of particles which will affect the fluidized bed pressure drop.

2.3 Results and Discussion

The empty column differential pressure drop is shown in Figure 2.3. This empty column pressure drop consists of the resistance due to the column and the liquid distributor. This

pressure drop is subtracted from the pressure drop data obtained from the inverse fluidized bed of aerogel granules to obtain the pressure drop due to the bed of particles.

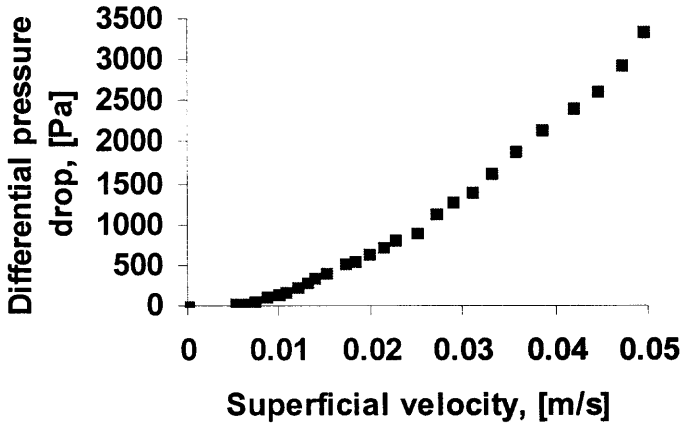

Figure 2.3 Pressure drop across the empty column.

The fluidized bed pressure drop and the bed height are the two most important parameters which contribute to the hydrodynamic characteristics of the inverse fluidized bed.

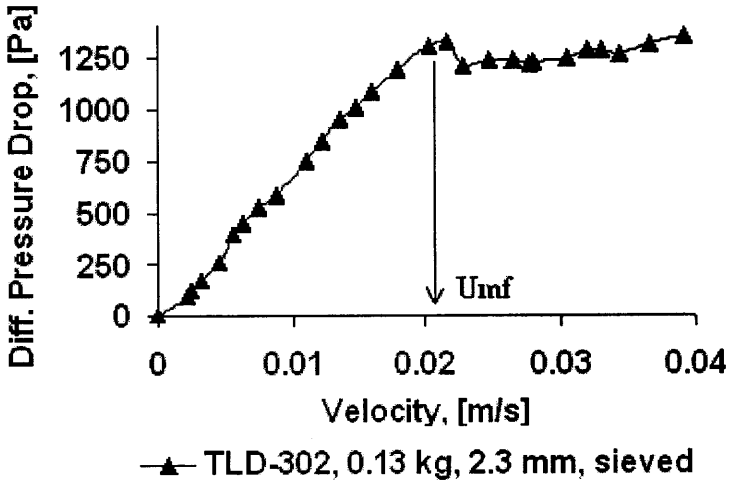

Figure 2.4 A typical plot of the inverse fluidized bed pressure drop.

A typical plot of superficial velocity against bed pressure drop of inverse fluidized bed of particles is shown in Figure 2.4. Figure 2.4 is plotted from the data obtained by inversely fluidizing 130 gm of TLD 302 Nanogel® (1.7 – 2.3 mm). The plot shows that the pressure drop rises proportionally to the fluid velocity and then at a certain velocity of the fluid, it becomes constant. The velocity at which the pressure drop of the bed of particles becomes constant is the minimum fluidization velocity (U_{mf}). At this point the weight of the bed due to gravity plus the drag force due to the flow of fluid exactly equals the buoyancy force of the particles. Thus, this plot gives two important parameters, namely, the minimum fluidization velocity and the constant pressure drop after the bed is fully fluidized. The values of U_{mf} will be calculated using available models in the literature and compared to the experimental results.

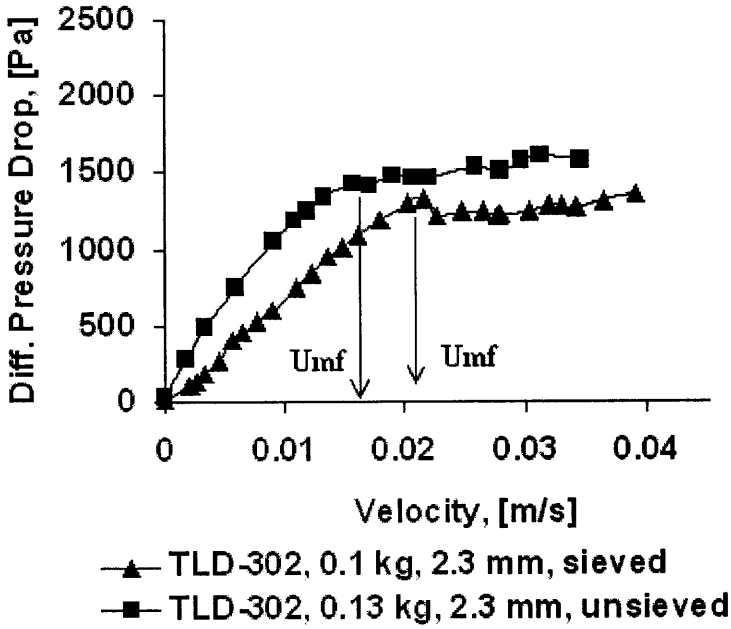

Figure 2.5 Difference in U_{mf} and pressure drop due to sieving and not sieving the particles.

Figure 2.5 shows clearly the difference between the pressure drop data of TLD 302 granules with sieving and not sieving them. Since unsieved granules have particles greater than 2.3 mm and less than 1.7 mm along with the particles between 1.7 – 2.3 mm, the pressure drop of the bed is affected. The minimum fluidization velocity is shifted to a higher value.

In Figure 2.6 it is seen that the particles having the same size have the same U_{mf} irrespective of the amount of mass used. The same figure also shows that the bed pressure drop depends on the amount of granules used which means that a greater mass of granules will have a greater pressure drop.

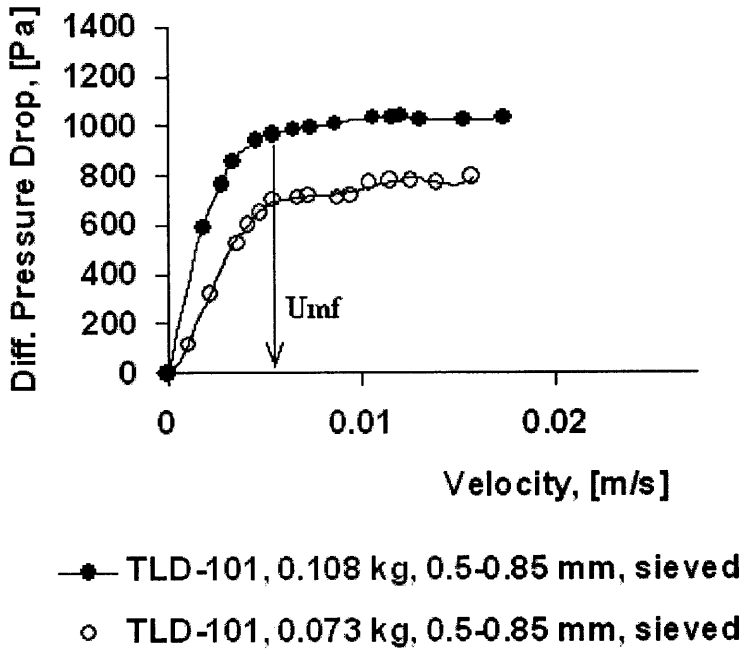

Figure 2.6 A plot showing that U_{mf} does not change by changing the amount of granules.

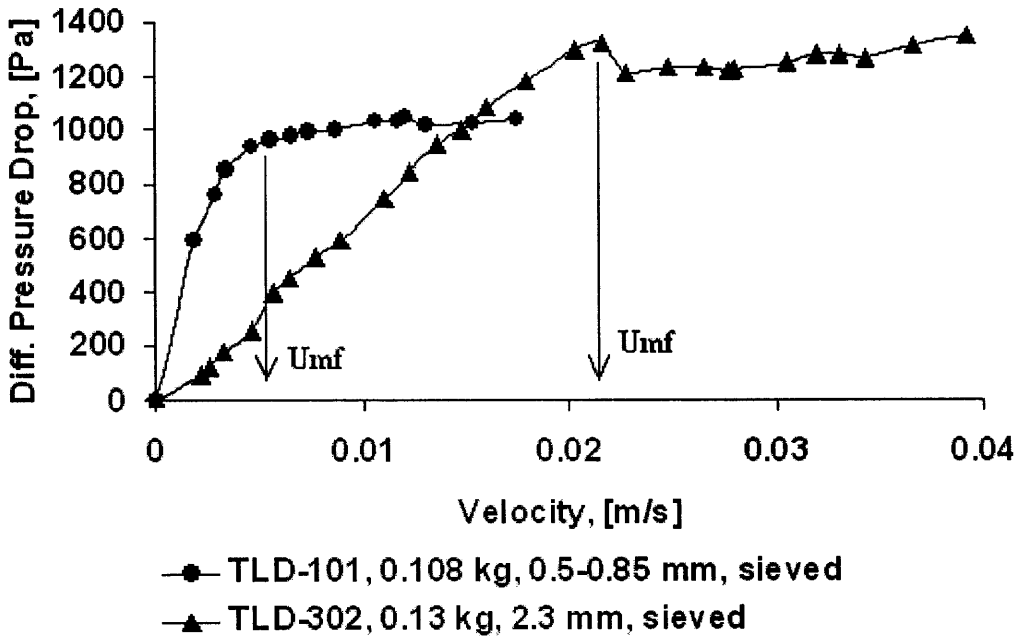

Figure 2.7 Change in U_{mf} with a change in granule size.

But if the size of the particles used for inverse fluidization is changed then, the U_{mf} will also change as shown in Figure 2.7. This figure shows that larger granules have larger minimum fluidization velocity as compared to the smaller granules.

Another important point to take into consideration is elutriation or entrainment or carryover of particles with the flow of water. Elutriation can be contained by increasing the flow of water gradually and sieving the granules properly before loading them into the column.

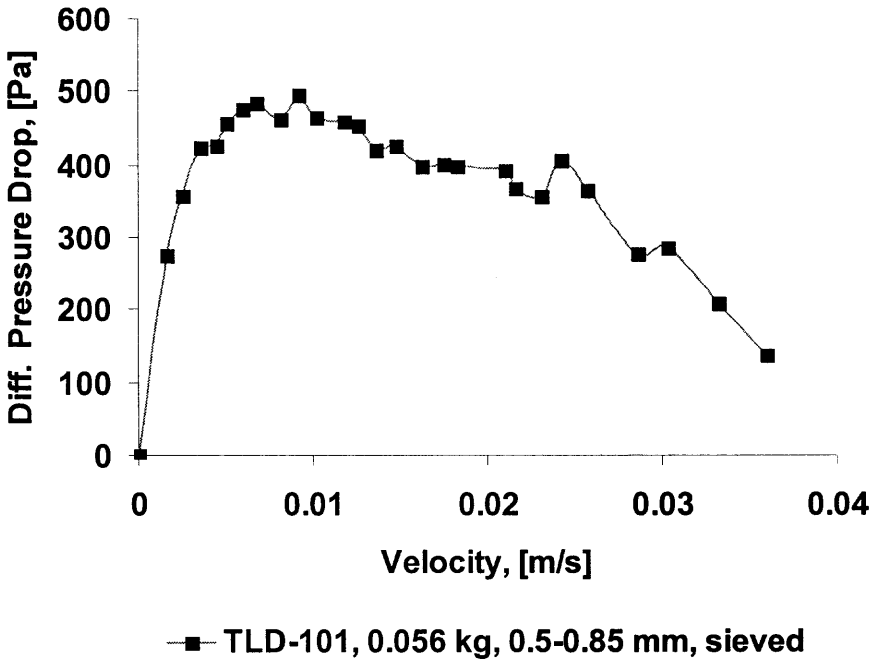

Figure 2.8 Effect of entrainment on the bed pressure drop.

Figure 2.8 shows the affect of elutriation on the pressure drop characteristics of the inverse fluidized bed of aerogel granules; it shows that initially when there is no elutriation the pressure drop increases as expected but once the elutriation starts, the total weight of the particles decreases and therefore the bed pressure drop also decreases. When this happens, the bed height and pressure drop data obtained are no longer useful for studying the hydrodynamic characteristics.

A plot of the fluidized bed height of different amounts of particles of the same size is shown in Figure 2.9; it indicates that the bed expansion obtained with 1.7 to 2.3 mm particles is more than 1.5 times the static bed height in the velocity range from 0 -5 cm/s.

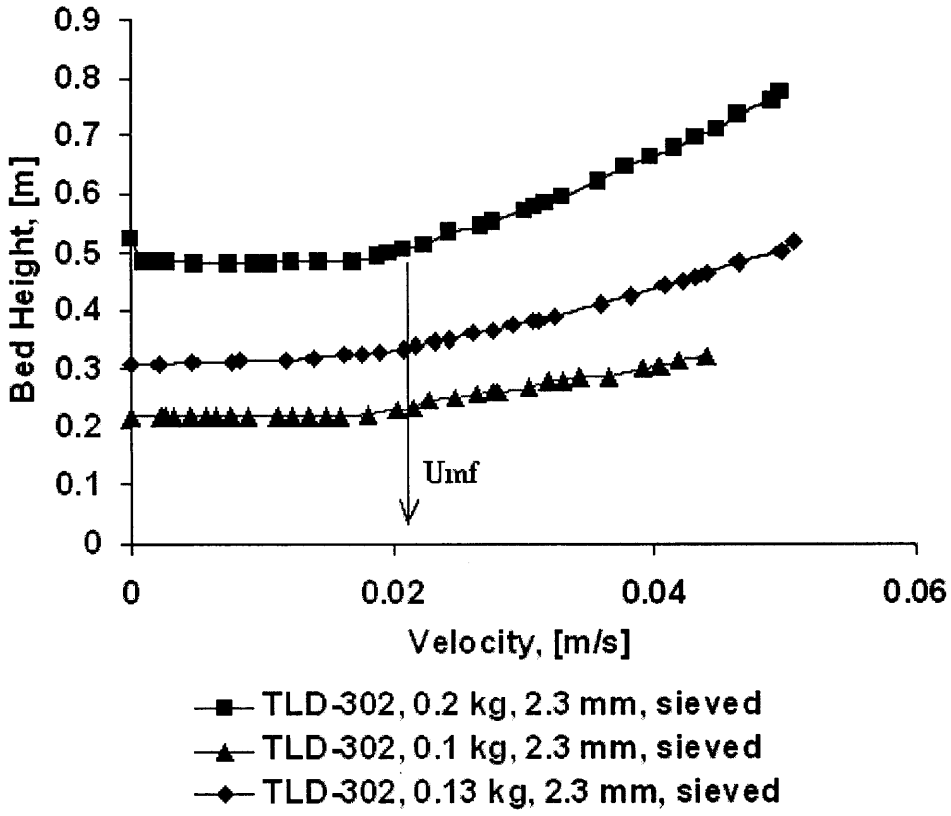

Figure 2.9 Bed expansion with different amount of granules of the same size.

Another plot of bed expansion of two different sizes of particles is shown in Figure 2.10. This figure shows that particles of smaller size give a larger bed expansion which is about 3 times the static bed height. This experimental bed expansion data is used in the determination of the theoretical size of the granules by using the Richardson-Zaki model and will be compared to the measured granule size. The U_{mf} and the estimated granule size data are very important because no previous experiments on finding the hydrodynamic characteristics of the aerogel granules in a solid-liquid inverse fluidized bed have been done.

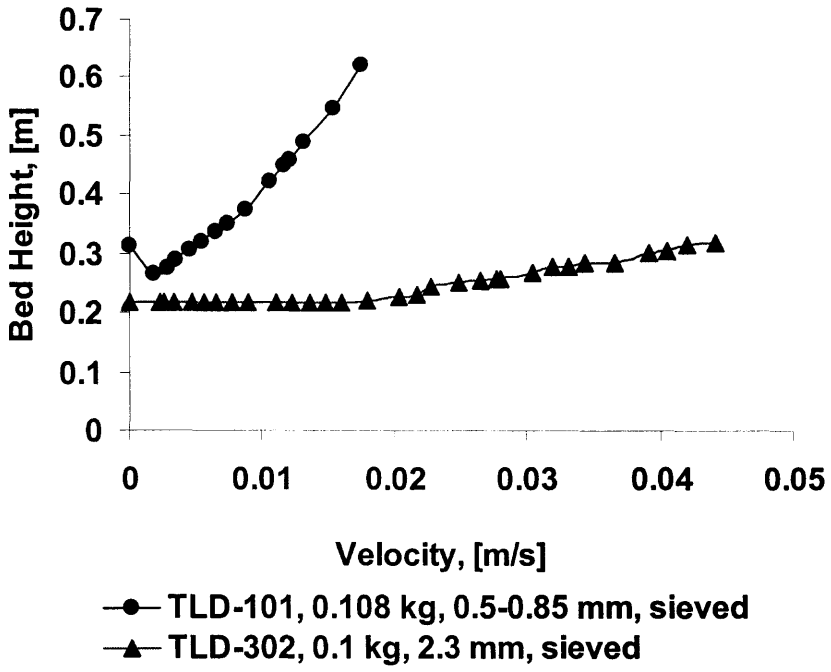

Figure 2.10 Bed expansion with two different size of granules of comparable mass.

2.3.1 Determination of the Granule Density (ρ_p) and the Internal Porosity (ε_p) of the Granule from the Experimental Data

The determination of the granule density is important because it is used in the calculation to find the void fraction of the fluidized bed. Once the granules are fluidized there is equilibrium between the forces acting on it.

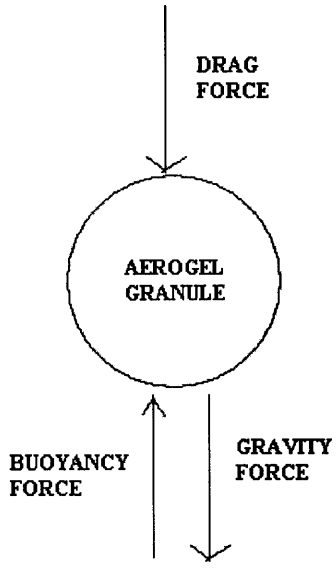

Figure 2.11 Schematic of an aerogel granule with the forces acting on it.

These forces are basically gravity, buoyancy and drag forces. Figure 2.11 shows the direction of forces acting on the aerogel granules.

The mass of the particles is given by

$$m_p = \rho_p V_p \tag{2.1}$$

The buoyancy force is given by

$$F_B = \rho_l V_P g \tag{2.2}$$

while the gravity force can be expressed as

$$F_g = \rho_p V_p g \tag{2.3}$$

Placing Equation 2.1 in Equation 2.3 gives

$$F_g = m_p g \tag{2.4}$$

and the drag force is represented by the classical drag equation

$$F_D = \frac{1}{2} C_D \rho_l U_{mf}^2 \left(\frac{\pi}{4}\right) d_p^2 \tag{2.5}$$

Since the gravity and drag forces act downwards and the buoyancy force acts upwards in an inverse fluidized bed of particles, a force balance on the particles will gives

$$F_B = F_g + F_D \tag{2.6}$$

The drag force acting on the particles during fluidization is also represented by the experimental pressure drop times the cross sectional area of the fluidization column

$$F_D = \Delta P_{\exp} A \tag{2.7}$$

Replacing Equations 2.2, 2.4 and 2.7 into Equation 2.6 gives

$$m_p g + \Delta P_{\exp} A = \rho_l V_P g \tag{2.8}$$

and by solving for V_P gives

$$V_p = \frac{\left(\Delta P_{\exp} A + m_p g\right)}{\rho_l g} \tag{2.9}$$

The void volume of the packed bed or fluidized bed (V_ε) is the difference between the total volume of the packed bed or fluidized bed (V_b) and the total volume of the particles given by Equation 2.10

$$V_\varepsilon = V_b - V_p \tag{2.10}$$

The porosity or void volume of the bed is the ratio of the void volume to the total volume of the bed so that

$$\varepsilon = \frac{V_\varepsilon}{V_b} \tag{2.11}$$

The total volume of the bed is easily calculated by multiplying the cross sectional area of the fluidization column with the height of the bed of particles

$$V_b = AH \tag{2.12}$$

Therefore, once the voidage of the bed is calculated, the solid fraction of the bed can also be calculated by

$$\phi = 1 - \varepsilon = \frac{V_p}{V_b} \tag{2.13}$$

The initial bulk density of the bed as shown in Table 2.1 is given by

$$\rho_{b0} = \frac{m_p}{V_{b0}} = \frac{m_p}{AH_0} \tag{2.14}$$

and the bulk density of the fluidized bed is

$$\rho_b = \frac{m_p}{V_b} = \frac{m_p}{AH} \tag{2.15}$$

The bulk density of the fluidized bed changes with the fluidized bed height which in turn changes with the velocity of the liquid. The total mass of the particles used in a particular experiment is known because, before adding the particles in the fluidization column, they are weighed accurately. Moreover, the total volume of the particles can be calculated by Equation 2.10. Therefore, the density of the particle can be calculated by

$$\rho_p = \frac{m_p}{V_p} \tag{2.16}$$

The internal porosity of the particles can be found by the following equation

$$\varepsilon_p = 1 - \frac{\rho_p}{\rho_s} \tag{2.17}$$

The aerogel granule density (ρ_p) is used to calculate the void fraction of the fluidized bed which in turn is used in the Richardson-Zaki correlation for the estimation of the terminal velocity and the size of the granule. Some results of the calculation of the aerogel granule density and the respective void fraction of the bed using the equations derived above are summarized in Table 2.1.

Table 2.1 Calculation of the Granule Density and the Initial Void Fraction from Experimental Data

Run	Granule Size/Type	Mass	ΔP (exp.)	ΔP (theo.)	Particle Volume	ρ_p (estim.)	Initial Bed Height	Bulk Density	Void Fraction
#	mm/type	kg	Pa	Pa	m3	kg/m3	m	kg/m3	ε_0
1	0.5 - 0.85 TLD 101	0.108	1310	1047	9.57E-04	112.9	0.2635	66.031	0.41
2		0.056	620.5	646	4.58E-04	122.2	0.1286	70.154	0.43
3		0.056	620.5	520	4.58E-04	122.2	0.146	61.793	0.49
4		0.056	675.7	653	4.94E-04	113.4	0.154	58.583	0.48
5		0.072	813.6	780	5.99E-04	120.1	0.1825	63.559	0.47
6	1.7 - 2.3 TLD 302	0.197	2089	2000	1.55E-03	127	0.4841	65.56	0.48
7		0.098	1034	1200	7.68E-04	127.5	0.2159	73.127	0.43
8		0.13	1413	1455	1.05E+00	124.3	0.3063	68.376	0.45
9	0.5 - 2.3 TLD 302	0.129	1482	1312	1.09E-03	118.4	0.3222	64.501	0.46
10		0.129	1448	1480	1.07E-03	120.9	0.3127	66.461	0.45

2.3.2 Richardson-Zaki Analysis to Find the Terminal Velocity (U_t) and to Estimate the Granule Size (d_p)

The Richardson–Zaki correlation (Richardson and Zaki., 1954) shown in Equation 2.18 is used to find the terminal velocity and the size of the fluidizing particles/granules.

$$\varepsilon^n = \frac{U}{U_i} \tag{2.18}$$

In the above equation the superficial velocity (U) and the settling velocity of the granule at infinite dilution (Ui) are a function of the void fraction to the nth power. Some empirical correlations to find the Richardson-Zaki index (n) as a function of the particle terminal Reynolds number (Re_t) and the particle to column diameter ratio are given below (Gupta et al., 1999)

$$n = \left(4.4 + 18\frac{d_p}{D}\right) \mathrm{Re}_t^{-0.1} \quad \text{for } 1<\mathrm{Ret}<200 \tag{2.19}$$

$$n = 4.4\,\mathrm{Re}_t^{-0.1} \quad \text{for } 200<\mathrm{Ret}<500 \tag{2.20}$$

$$n = 2.4 \quad \text{for Ret}>500 \tag{2.21}$$

The Richardson-Zaki exponent (n) can also be obtained by experimental data by plotting the logarithm of the superficial velocity against the logarithm of the void fraction

$$\ln(U) = n\ln(\varepsilon) + \ln(U_i) \tag{2.22}$$

When Equation 2.22 is plotted, a slope which is equal to n and a y-intercept which is equal to the logarithm of (U_i) is obtained. Thus, the settling velocity of the granule at infinite dilution can be easily obtained. In order to get the values of the void fraction (ε), Equation 2.13 is used.

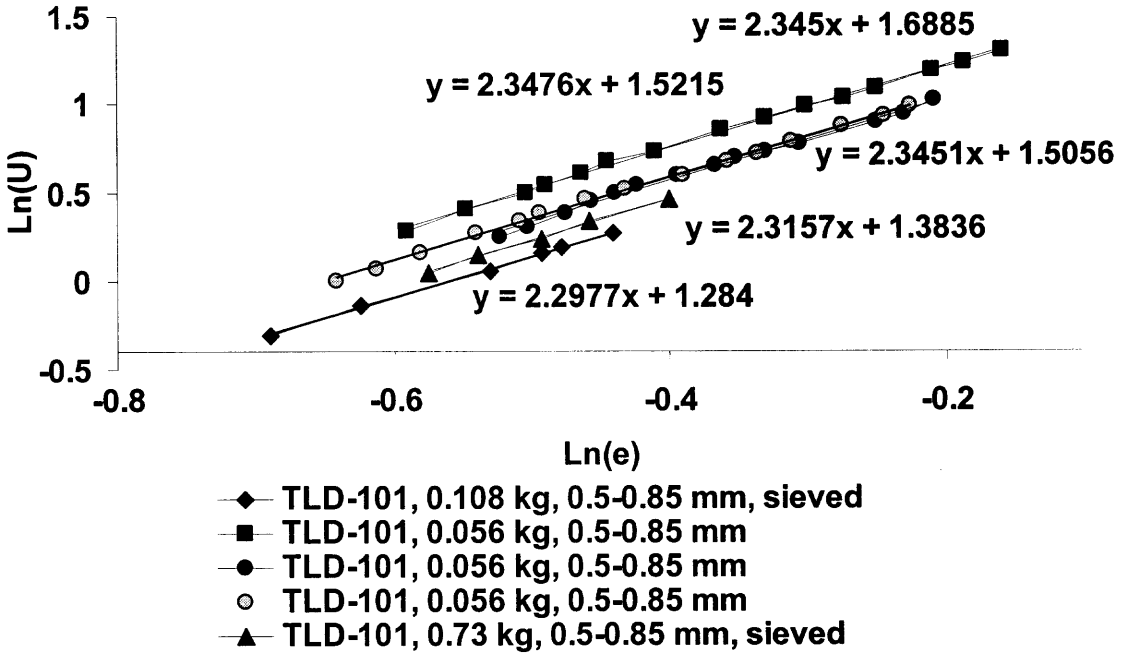

Figure 2.12 Relationship between the superficial velocity and the void fraction of inverse fluidized beds of aerogel granules of the type TLD 101.

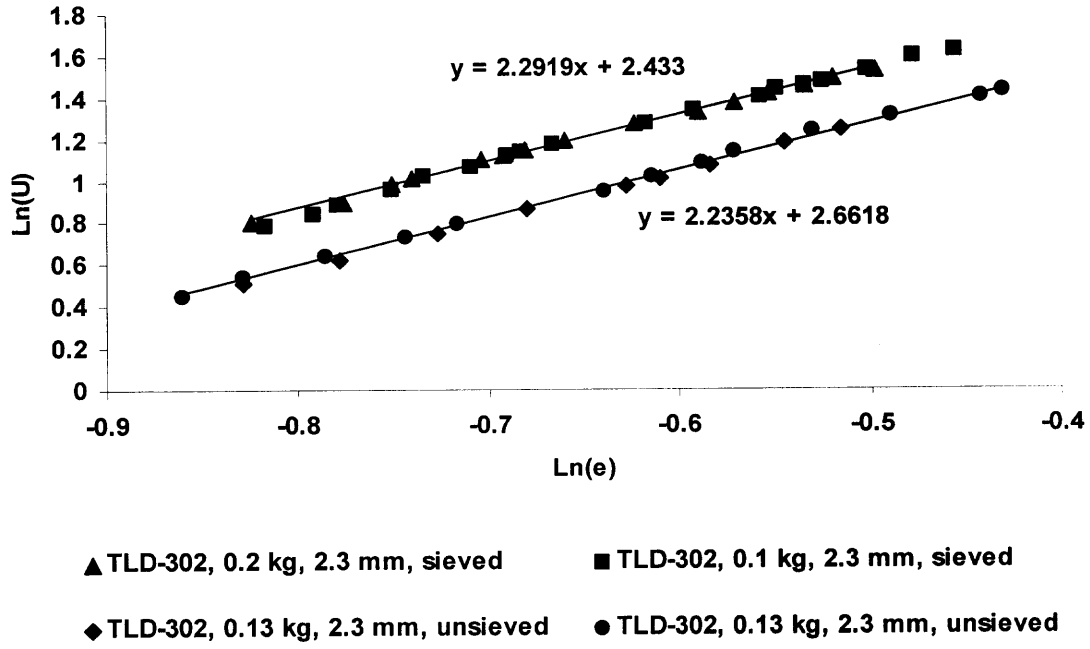

Figure 2.13 Relationship between the superficial velocity and the void fraction of inverse fluidized beds of aerogel granules of the type TLD 302.

Figures 2.12 and 2.13 show the plot between *ln*(U) and *ln*(ε) for different experiments conducted during inverse fluidization of aerogel granules (TLD 101 and TLD 302). From these plots, the corresponding Richardson-Zaki exponent (n) and the settling velocity (U_i) are obtained for each experiment.

The settling velocity (U_i) and the terminal velocity (U_t) are related by

$$\log U_i = \log U_t - \frac{d_p}{D} \tag{2.23}$$

where U_t is given by the equation below according to Sakiadis (1984),

$$U_t = \sqrt{\frac{4(\rho_l - \rho_p) g d_p}{3 \rho_l C_d}} \tag{2.24}$$

where C_d is the drag coefficient which is a function of the particle Reynolds number.

Assuming the granules to be spherical, the following correlations can be stated for finding C_d (Gupta et al., 1999)

$$C_d = 24 / \mathrm{Re}_p \qquad \text{for Rep<0.1} \tag{2.25}$$

$$C_d = (24 / \mathrm{Re}_p)(1 + 0.14 \mathrm{Re}_p^{0.70}) \qquad \text{for Rep<1000} \tag{2.26}$$

$$C_d = 0.445 \qquad \text{for 1000< Rep<350000} \tag{2.27}$$

$$C_d = 0.19 - [(8)(10^4) / \mathrm{Re}_p] \qquad \text{For Rep>}10^6 \tag{2.28}$$

The particle Reynolds number is given by

$$\mathrm{Re}_p = \frac{U \rho_l d_p}{\mu_l} \tag{2.29}$$

Using the experimental data and the above equations, the Richardson – Zaki exponent (n), the terminal velocity (U_t) and the particle diameter (d_p) were calculated and

listed in Table 2.2. Since the Re_p calculated from Equation 2.29 had a range between 4 to 100, Equation 2.26 was used to find the C_d. The terminal velocity of the granule (U_t) was calculated by Equation 2.23. The granule diameter (d_p) in Table 2.2 was calculated by rearranging Equation 2.24 and solving for d_p.

Table 2.2 Richardson-Zaki Bed Expansion Parameters and Calculation of the Particle Size from Experimental Data

Granule Size/Type mm/type	d_{p0} m	Re_p	Cd (Eq. 2.26)	R-Z "n"	R-Z "ln(Ui)"	Ut (Eq. 2.23) m/s	d_p (Eq. 2.24) m
0.5 - 0.85 TLD 101	0.0008	10.63753	4.246581	2.33022	1.47664	0.04517	0.00070
1.7 - 2.3 TLD 302	0.0022	63.99315	1.116306	2.2572	2.7225	0.16179	0.00252
0.5 - 2.3 TLD 302	0.002	44.96458	1.607294	2.30405	2.46755	0.12520	0.00215

From the data shown in Table 2.2, it can be said that the Richardson-Zaki model can correctly predict the size of the granule with little error. The error may be due an inaccuracy of sieving the granules and to the effect of the particle size distribution.

2.3.3 Comparison of Experimental and Calculated Minimum Fluidization Velocity

Wen and Yu (1966) proposed an empirical correlation to find the minimum fluidization velocity based on the force balance. The equation suggested by Wen and Yu is given below

$$\mathrm{Re}_{mf} = \sqrt{(33.7)^2 + 0.0408 Ar} - 33.7 \qquad (2.30)$$

which was introduced by Wen and Yu (1966).

This equation is not only applicable to conventional upflow fluidized beds but also for the inverse fluidized bed as suggested in the literature (Renganathan et al., 2003). The basic principle for finding the minimum fluidization velocity is that the net buoyancy force per unit area is balanced by the pressure drop across the bed at minimum fluidization. The experimental minimum fluidization velocities of the aerogel granules found by the differential pressure drop data can be compared with the U_{mf} resulting from Equation 2.30. Both the experimental and calculated U_{mf} data are shown in Table 2.3.

Table 2.3 Comparison of the Experimental and Theoretical Minimum Fluidization Velocities

Run #	Granule Size/Type mm/type	U_{mf} [1] m/s	d_p mm	Ar	Re_{mf}	U_{mf} [2] m/s	Error %	U_{mf} [3] m/s	Error %
1	0.5 - 0.85 TLD 101	0.00549	0.65	2.4E+03	1.4	0.0022	59.9	0.004	28.0
2		0.00523	0.75	3.7E+03	2.1	0.0029	45.1	0.0053	0.33
3		0.00610	0.7	3.0E+03	1.8	0.0025	58.7	0.0045	12.33
4		0.00718	0.7	3.0E+03	1.8	0.0025	64.7	0.0046	36.2
5		0.00541	0.7	3.0E+03	1.8	0.0025	53.4	0.0046	15.95
6	1.7 - 2.3 TLD 302	0.01962	2.6	1.5E+05	51.9	0.0201	-2.3		
7		0.01799	2.6	1.5E+05	51.9	0.0201	-11.5		
8		0.01763	2	6.9E+04	29.2	0.0147	16.8		
9	0.5 - 2.3 TLD 302	0.01496	2.2	9.2E+04	36.4	0.0166	-11.0		
10		0.01567	2.2	9.2E+04	36.4	0.0166	-6.0		

1: From experiments
2: Wen and Yu correlation
3: Frantz correlation

It is seen from the table that a larger error results for the prediction of minimum fluidization velocity of smaller particles by the Equation 2.30. This error is reduced if the Frantz correlation (Gupta et al., 1999) based on the drag force principle is

applied to find the theoretical minimum fluidization velocity. The general form of Frantz correlation is:

$$\mathrm{Re}_{mf} = K_2 Ar \tag{2.31}$$

where, K_2 is 1.065×10^{-3} for $\mathrm{Re}_{mf} < 32$.

The experimental minimum fluidization velocity could also be used to find whether the fluidized bed system is particulate or aggregative. A dimensionless correlation was given by Wilhem and Kwauk (Gupta et al., 1999) for checking the quality of fluidization. The correlation states that if the minimum fluidization Froude number Fr_{mf} is less than 0.13 than the fluidization will be particulate (smooth) and if the Froude number is greater than 0.13 then the fluidization is aggregative (bubbling). The Fr_{mf} is given as follows:

$$Fr_{mf} = \{U_{mf}^2/(d_p.g)\} \tag{2.32}$$

From Table 2.3, the experimental minimum fluidization velocities (U_{mf}) and the particle density (d_p) were used in the Equation 2.32 which gave a Fr_{mf} ranging from 1.6×10^{-5} to 0.007. These Fr_{mf} values are well below 0.13, which means that the inverse fluidization of the aerogel granules, with the size range from 0.5 – 0.85mm and 1.7 – 2.3 mm, show particulate behavior. This smooth inverse fluidization behavior can also be seen by visually observing the fluidized bed of these particles.

CHAPTER 3

OIL REMOVAL USING INVERSE FLUIDIZED BED OF NANOGEL

3.1 Introduction

There are number of ways by which the water is polluted with oil or hydrocarbons. Some examples include stormwater runoffs, oil spill from an oil tanker into an ocean, hydrocarbon waste generated from oil refineries, sewage water from household, waste generated from metal cutting fluids, used motor oil and many more. This polluted water can enter into oceans, rivers, and ground water and ultimately contaminating them.

A study by the American Petroleum Institute (API) describes that more than 15% of the used oil generated in the U.S. yearly is not collected. This huge amount of oil (nearly 200 million gallons/year) is usually dumped into the drains, streams, sewers, landfills and backyards. This dumping could easily contaminate under water drinking sources and rivers and can lead to problems related to human health. Moreover, it can also create a danger for the aquatic life.

One of the major sources of oil release are petroleum and petrochemical plants which generate a huge amount of oil-based waste products which should be treated before dumping them into the natural water bodies (Johnson et al., 1973). Other industries producing large amount of waste oil include the steel manufacturing and metal working companies which use oil containing metal-working fluids (Paterson, 1985). Municipal wastewater is also one of the major sources of oily substances containing up to 36% of oily material derived from vegetable oils and animal fats (Quemeneur et al., 1994).

One of the oldest techniques to remove oily wastes from water is using granulated activated carbon (GAC) as the media to adsorb the oil. Activated carbon is used for the adsorption of oil from water because of its highly porous structure and a large internal as well as external surface area for the molecules to get adsorbed. It is well known that silica aerogels, such as Cabot Nanogel®, are also very porous and have a large surface area. Some experiments performed at Lawrence Livermore National Laboratory (Livermore, CA) show that aerogels are capable of absorbing common pollutants like chlorobenzene or trichloroethylene 130 times more efficiently compared to granulated activated carbon (GAC). It has also been reported that efficiency of aerogels is far better than GAC for removing contaminants from water (Hrubesh et al., 2004). Since aerogels are hydrophobic, they do not allow water to enter into the nanopores, and the organic compounds which have lower surface energies and higher volatility enter the pores as a liquid or a gas and get easily absorbed. Thus, this high absorption capacity of aerogels, such as Nanogel® can prove to be a very important application for the removal of organic compounds such as oil from water.

An extensive description of aerogels is given by the Lawrence Berkeley National Laboratory (Ayres et al., 2004) and the Lawrence Livermore National Laboratory. An example of the effectiveness of aerogel in removing oil from water is as shown in Figure 3.1. In this figure it is clearly seen that when there is 10 or 30% GAC/Aerogel composite added to the crude oil-water mixture, the oil is adsorbed by the composite and clear water appears at the bottom.

Figure 3.1 The four bottles contain 0, 1.5, 10, and 30% GAC/Aerogel composite respectively in a crude oil water mixture.

As it is already discussed earlier, if the filtration is carried out using granular materials in a packed bed system, it has two disadvantages, a high pressure drop which increases as the flow rate of influent increases and a decrease in bed voidage as the filter gets saturated. Both of these factors adversely affect the operation of the packed bed filter resulting in a lower removal capacity.

Therefore, inverse fluidization was tested to check the applicability of aerogel granules in removing oil from water. As mentioned earlier, inverse fluidization was used because it has many advantages such as a low pressure drop, continuous operation, no reduction in bed voidage; therefore a higher removal efficiency and capacity. Another important advantage is that inverse fluidization also adds gravity separation along with the absorption of oil by the aerogels, thus combining two techniques in one unit operation. Since the oil droplets have a lower density compared to water, the oil-water mixture entering the column from the top is separated due to the density differences of the two fluids. This advantage makes the inverse fluidized bed of aerogels very attractive method to remove oil from water. The aerogel used in the present work was hydrophobic aerogel,

Nanogel® from Cabot Corporation, and the granule sizes tested were 0.5 to 0.85 mm and 1.7 to 2.3 mm.

3.2 Experimental Setup and Procedure

The experimental setup used for removal of oil from water was the same that was used for determining the hydrodynamics in the inverse fluidization of aerogel above. The changes made in the setup included a tap for the insertion of oil into the system, a static mixer and two other taps for inlet and outlet sampling of water. Among the fluidization characteristics monitored during the removal of oil from water are the pressure drop and the bed height. Also, the concentration of oil was monitored by analyzing the chemical oxygen demand at several time intervals during the experiment.

The experimental procedure was as follows. Vegetable oil (soybean oil) from a 1 gallon container was injected into a 1 inch PVC pipe by a Pulsatron Series A Plus diaphragm pump (0 – 6 Gallons/Day). The injected oil was then passed through the static mixer made of steel wire mesh packing which was incorporated into the PVC pipe. The function of the static mixer was to create small droplets of oil in water. This oil water mixture was then allowed to pass through the inverse fluidized bed of aerogel granules. The fluidized bed was kept at constant flow rate of water and the hydrodynamic characteristics such as pressure drop and bed height were measured in order to study the fluidization characteristics along with the oil removal. Samples of about 500 ml were collected at regular intervals from two sampling points before and after the fluidized bed,

respectively. The amount of oil entering into the system was adjusted through the stroke and frequency adjustment knobs on the diaphragm pump.

The samples taken were then analyzed for their chemical oxygen demand (COD) content. COD analysis is a well known technique to check the organic content of water. The COD content of normal tap water was found to be about 10 mg/l. Since oil was the only organic matter added to the water, it was assumed that any increase in COD level is due to the oil present in water. COD was measured by using a HACH DR/890 Colorimeter, and Method 8000: Reactor digestion method USEPA approved for COD (Jirka et al., 1975) (Hach Co. Method., 2004) (Furrow, 2005) was used as the analysis method for finding the COD content of the samples. A relation (calibration curve) between the COD content of the samples containing a known amount of oil in water and the concentration of oil in the same sample was obtained and shown in Figure 3.2.

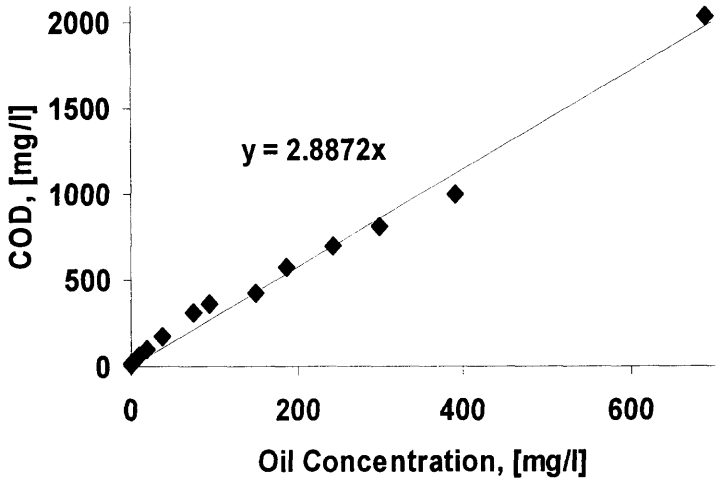

Figure 3.2 Correlation between the oil concentration in water and COD levels measured by HACH DR/890 Colorimeter.

This was done by taking a known volume of tap water, adding a known volume of oil in it and then doing its COD analysis. Similarly, the concentration of oil was increased

in the sample and tested for its COD content. Figure 3.2 shows the calibration curve which validates that the COD levels of a particular sample is proportional to the concentration of oil in water. The water samples taken from the experiment were blended thoroughly by using a Hamilton Beach (Model 50256MW) blender to disperse the oil droplets homogeneously. An aliquot of (2ml for 0 – 1500 mg/l COD and 0.2 ml for 0 – 15000 mg/l COD) was added to the COD digestion vial and kept into the digestion reactor at 150°C for 2 hours. After the digestion, the vial was allowed to cool down and then it was inserted into the Colorimeter to measure it COD content. The colorimeter has a digital display which showed the COD content of the sample in term of mg/l units.

In addition to using a colorimeter to check the concentration of oil, some other instruments and methods can be used such as the use of a TOC analyzer (Furrow, 2005) or a gravimetric analysis using a solvent like hexane or a spectrophotometer. However, this methods were not used here.

3.3 Results and Discussion

Different parameters were changed to check how the oil removal efficiency of the inverse fluidized bed of aerogel particles changes. For example variables like the particle size, initial bed height, flowrate of the fluid, concentration of oil entering the fluidized bed, and the amount of particles were changed. The process variables monitored during the experimental run where, fluid velocity, pressure drop, maximum bed expansion and the time at which the oil starts appearing in the effluent. Since the digital flowmeters used for the flow of water showed a reading in gallons/minute units, in order to convert these units into velocity (m/s), the flow rate was divided by the cross sectional area of the column.

The upstream oil concentration was adjusted using the two knobs present on the oil pump, one for the stroke frequency and another for the stroke length. The stroke length multiplied by stroke frequency and maximum output of the pump gave the total flow of oil entering the water stream.

This volume of oil divided by the volume of water entering the column accounted for the total concentration of oil entering the system. The concentration of oil downstream of the inverse fluidized bed was measured by taking a sample of 500 ml of liquid after the column but before the cartridge filter, as shown in Figure 2.2. The removal capacity of Nanogel was calculated as follows. First, the time duration for the first droplet of oil to appear below the bed of Nanogel (or the time when the downstream COD concentration reached a value of 100 mg/l) was noted. This time duration is the amount of time needed for the Nanogel to get saturated with oil. This time duration was multiplied by the flow rate of oil entering the fluidized bed system to give the amount of oil captured by the Nanogel, which was then divided by the weight of Nanogel used in the system. Thus the removal capacity of Nanogel in terms of kg of oil absorbed per kg of Nanogel was obtained.

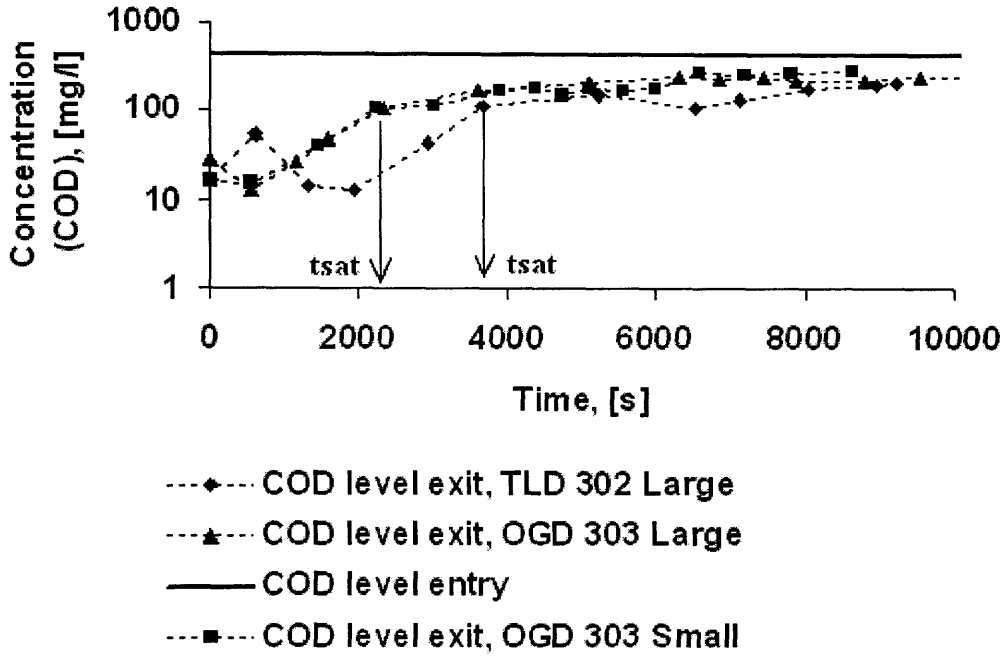

Figure 3.3 Chemical oxygen demand (COD) vs. time of 56 grams of aerogel granules (TLD 302 and OGD 303) with sizes between 1.7 to 2.3 mm (large) and 0.5 to 0.85 mm(small) during removal of oil from water (0.26 g of oil/kg of water and fluid velocity of 0.0305 m/s).

By visually observing the fluidized bed of aerogel particles it was found that as the particles started absorbing oil, they changed in color from translucent or white to yellowish suggesting that the yellowish colored vegetable oil is absorbing. Figure 3.3 shows 3 different plots of the COD level in the outlet stream of the inverse fluidized bed of TLD 302 (1.7 – 2.3 mm), OGD 303 (1.7 – 2.3 mm) and OGD 303 (0.5 – 0.85 mm). The operating conditions employed were as follows. The velocity of the oil-water mixture entering the system was kept constant at 0.03 m/s, mass of the Nanogel taken for each run was 0.056 kg, and the inlet COD concentration was kept at 450 mg/l. The time (tsat) in Figure 3.3 indicates the time required for the downstream concentration to reach a COD concentration of 100 mg/l. Since the tsat value (3660 sec) for the TLD 302 Nanogel is more than the tsat value for the other two types of Nanogel (2340 sec for large

OGD 303 and 2200 sec for small OGD 303), it is clear that the TLD 302 aerogel particles are better in terms of removal capacity. The removal capacity for TLD 302 (large), OGD 303 (large) and OGD 303 (small) was found to be 3.2, 2.0 and 1.9 kg oil/kg of Nanogel.

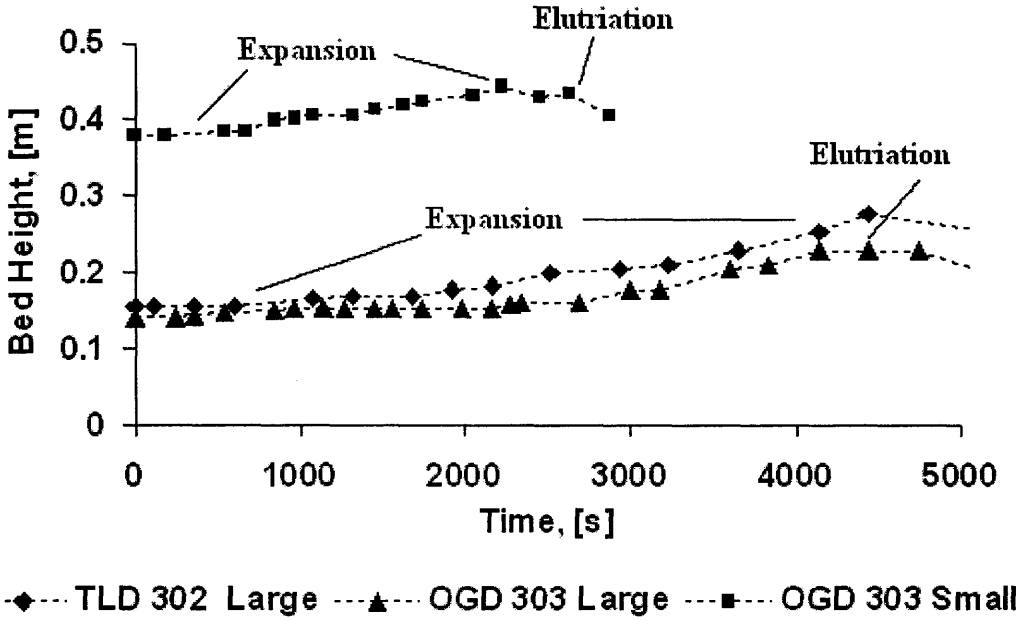

Figure 3.4 Bed expansion vs. time of 56 grams of aerogel granules (TLD 302 and OGD 303) with sizes between 1.7 to 2.3 mm (large) and 0.5 to 0.85 mm(small) during removal of oil from water (0.26 g of oil/kg of water and fluid velocity of 0.0305 m/s).

Figure 3.4 shows the bed expansion corresponding to the plots of Figure 3.3, where it is seen that the small OGD 303 have the largest bed expansion and the large TLD 302 particles have a slightly higher bed expansion compared to large OGD 303 particles. The initial expansion of the bed indicates that the particles are absorbing oil and becoming heavier which in turn leads to higher bed expansion. Once most of the particles are saturated with oil, the elutriation of those saturated aerogel particles starts and therefore the bed height also starts diminishing.

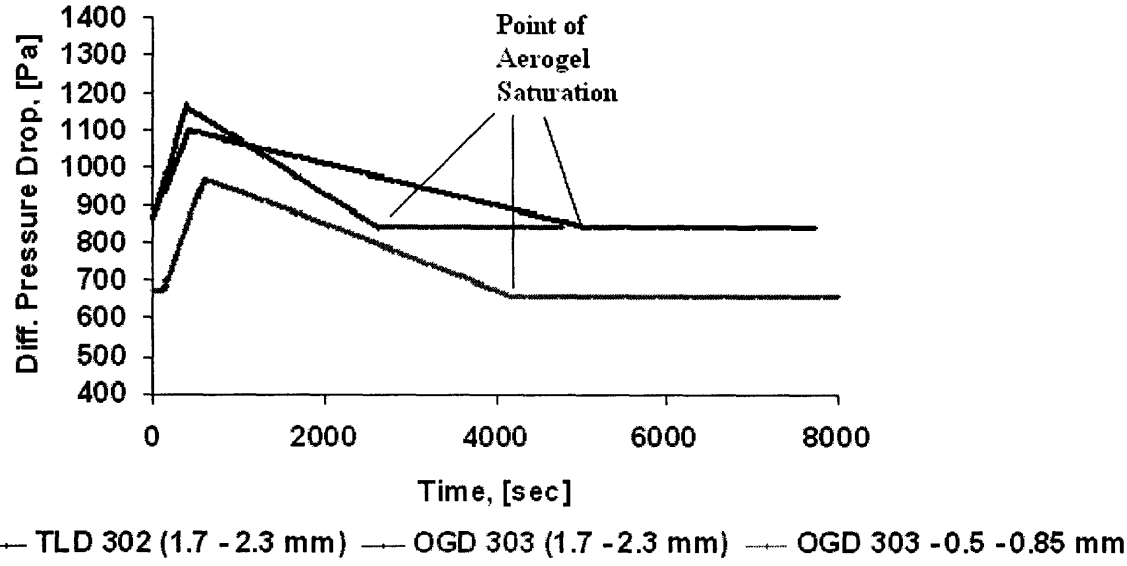

Figure 3.5 Pressure drop across the inverse fluidized bed of aerogel during the removal of oil corresponding to Figure 3.3. Superficial flow velocity was kept constant at 0.0305 m/s.

The pressure drop data for the plots in Figure 3.3 is shown in Figure 3.5. In this figure an interesting observation was that, as the oil was introduced into the inverse fluidized bed of particles, initially there was an increase in pressure drop and then it starts slowly decreasing, and towards the end becomes almost constant. The increase in pressure drop was due to the introduction of oil into the system. The decrease in pressure drop was because the aerogel granules were getting heavier after adsorbing oil subsequently reducing the drag force due to the reduced buoyancy. Moreover, entrainment of these heavy particles with the flow of water also causes lose of particles, which also contribute to the reduction in pressure drop.

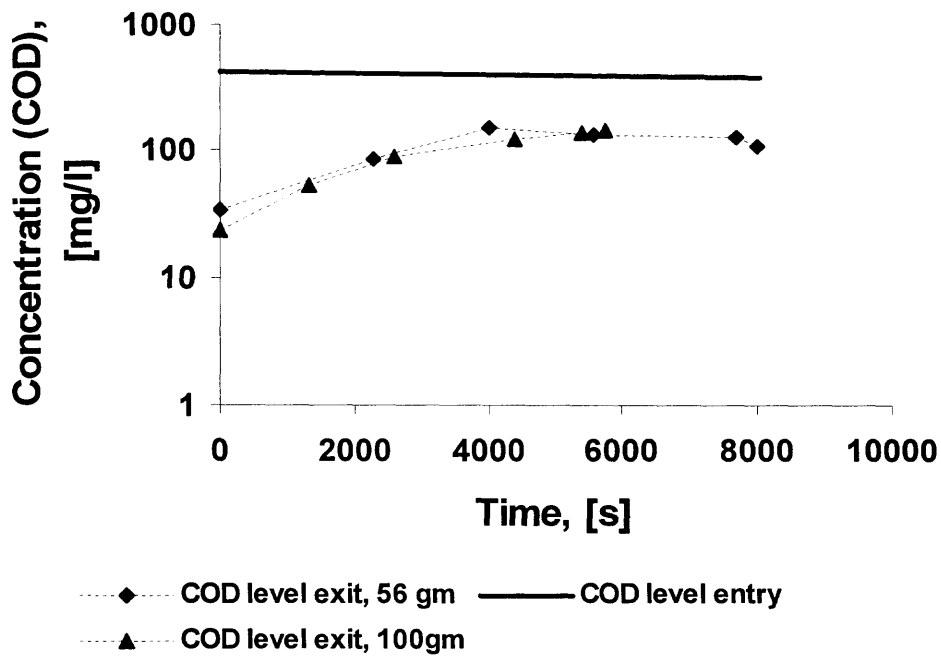

Figure 3.6 Chemical oxygen demand (COD) vs. time of 56 grams and 100 grams of aerogel granules (OGD 303) with sizes between 0.5 to 0.85 mm(small) during removal of oil from water (0.19 g of oil/kg of water and fluid velocity of 0.0305 m/s).

Figure 3.6 compares the effectiveness of two different amounts of the same aerogel granules keeping all other operating conditions same. The operating conditions employed for this experimental run were as follows. The granules used were OGD 303 (0.5 – 0.85 mm), the fluid velocity was 0.03 m/s, and the upstream COD concentration was 455 mg/l. It is clear from the figure that the removal capacity of the two different amounts of aerogel (0.056 kg and 0.10 kg) used in the experiment remained almost the same which indicates that the removal capacity mostly depends on the bed void fraction and the superficial velocity of the fluid. The removal capacity was found to be 1.8 kg of oil/kg of Nanogel.

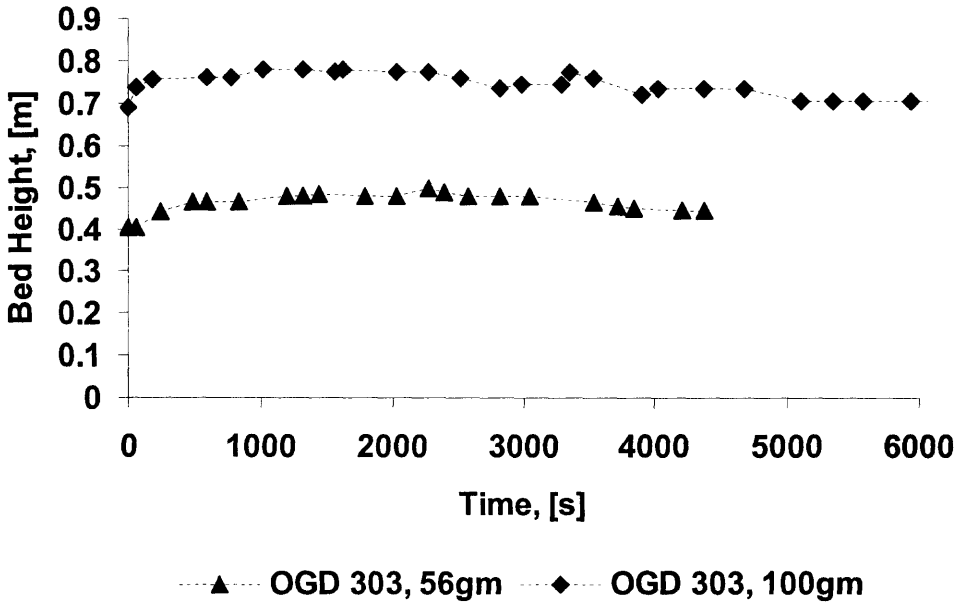

Figure 3.7 Inverse fluidized bed expansion as a function of time of 100 grams of aerogel granules (OGD 303) with sizes between 0.5 to 0.85 mm during removal of oil from water (0.19 g of oil/kg of water and fluid velocity of 0.0305 m/s).

The bed expansion plots corresponding to the Figure 3.6 are shown in Figure 3.7. It is observed that the bed expansion trend of both 56 gm and 100 gm of aerogel is quite similar which is due to the similar absorption behavior shown in Figure 3.6. The pressure drop data corresponding to the Figure 3.6 is shown in Figure 3.8, which again shows the same trend which was explained earlier in this section.

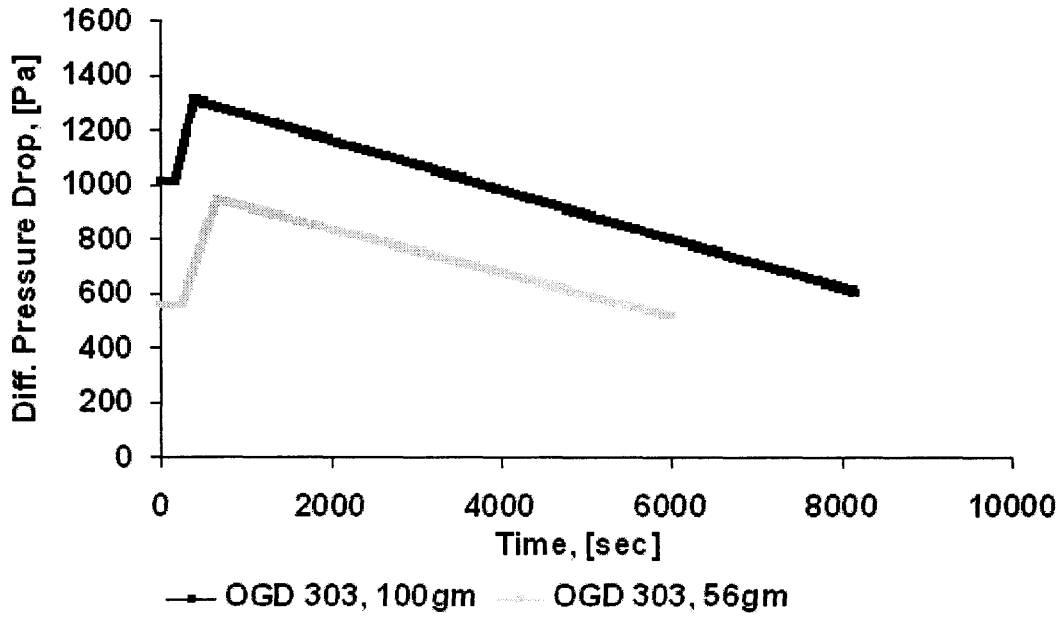

Figure 3.8 Pressure drop across the inverse fluidized bed of aerogel during the removal of oil corresponding to Figure 3.6. Superficial flow velocity was kept constant at 0.0305 m/s.

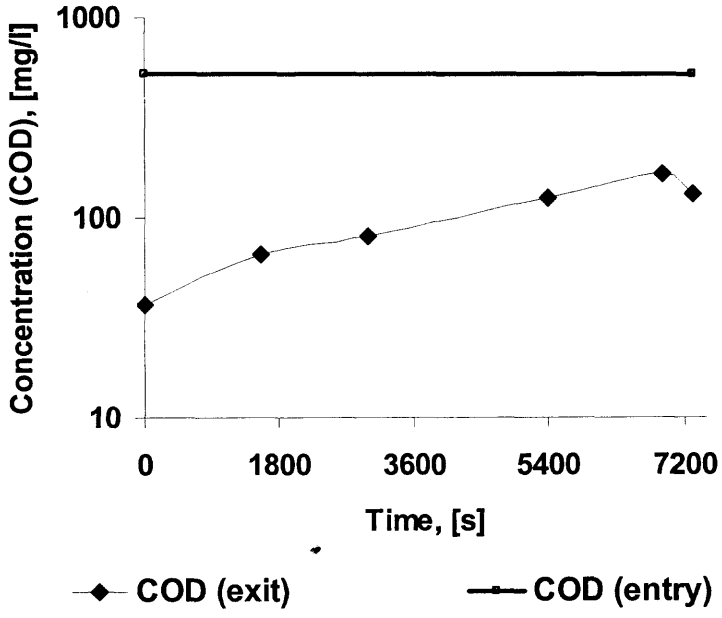

Figure 3.9 Chemical oxygen demand (COD) vs. time of 56 grams of aerogel granules (OGD 303) with sizes between 0.5 to 0.85 mm during removal of oil from water (0.17 g of oil/kg of water and 0.0248 m/s fluid velocity).

Another experiment was done to check the effects of two different concentrations of oil entering the inverse fluidized bed of OGD 303 (0.5 – 0.85 mm) aerogel granules. The operating parameters for this experiment were as follows. The fluid velocity was 0.025 m/s and the mass of aerogel was 0.056 gm. The two different inlet COD concentrations were 520 and 770 mg/l. As expected, by looking at the Figure 3.9 and Figure 3.10, the inverse fluidized bed of aerogel granules gets saturated faster when it is faced with a higher concentration of oil.

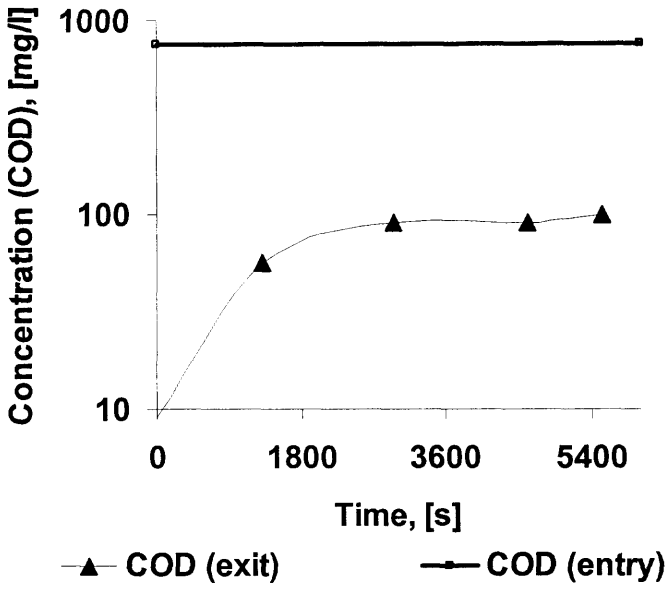

Figure 3.10 Chemical oxygen demand (COD) vs. time of 56 grams of aerogel granules (OGD 303) with sizes between 0.5 to 0.85 mm during removal of oil from water (0.36 g of oil/kg of water and 0.0244 m/s fluid velocity).

The faster saturation of the aerogel granules at higher inlet concentration of oil is also shown by Figure 3.11 and Figure 3.12. The bed height of the aerogel granules, facing a low concentration of oil, drops slowly as compared to the granules facing a high concentration of oil.

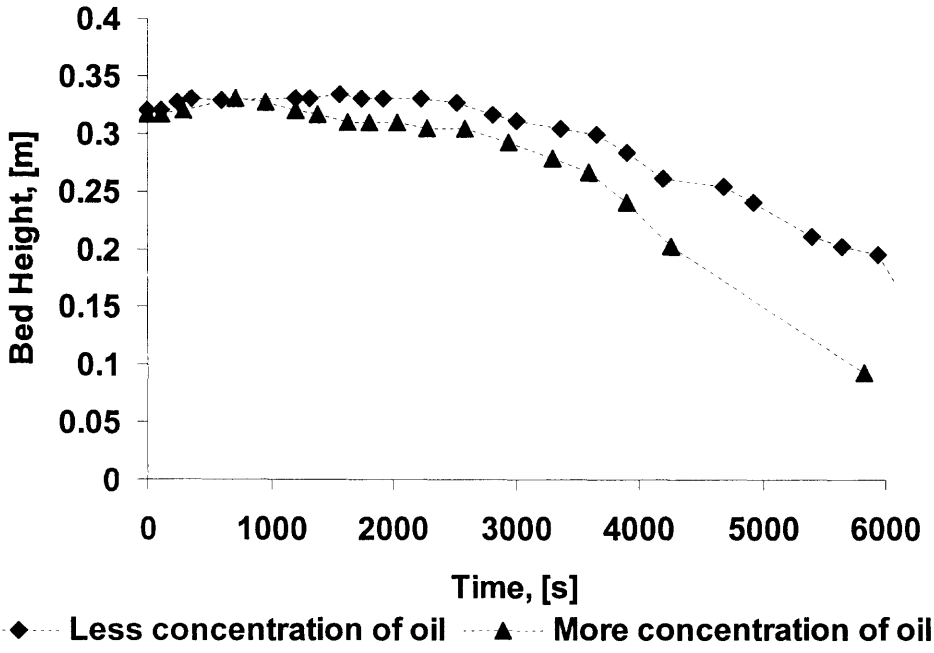

Figure 3.11 Inverse fluidized bed expansion vs. time of 56 grams of aerogel granules (OGD 303) with sizes between 0.5 to 0.85 mm during removal of oil from water corresponding to Figure 3.9 and 3.10.

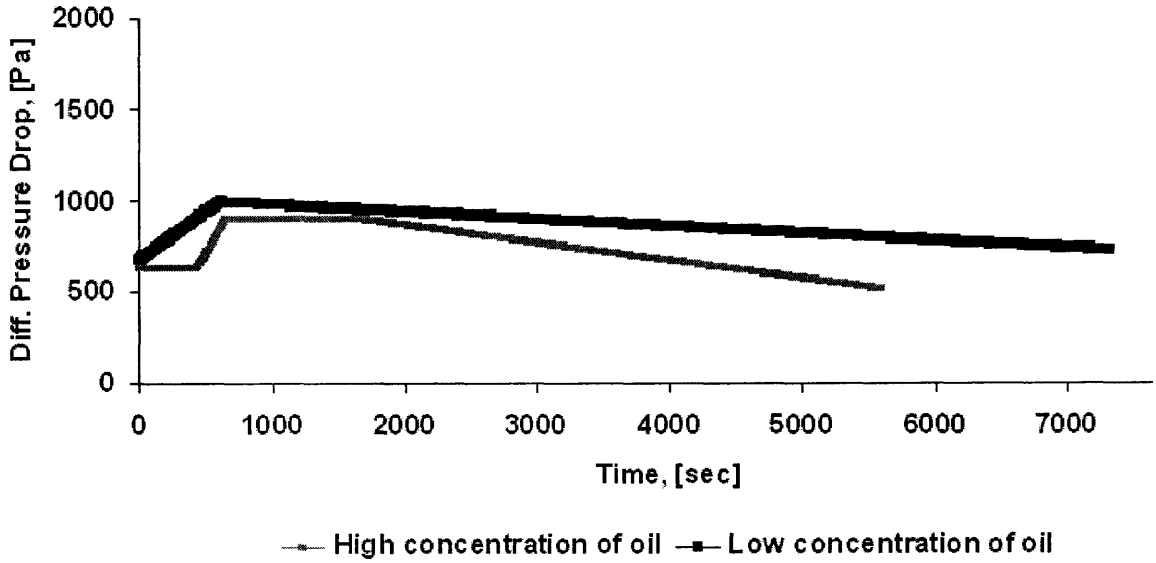

Figure 3.12 Pressure drop across the inverse fluidized bed of aerogel during the removal of oil corresponding to Figure 3.9 and 3.10. Superficial flow velocity was kept constant at 0.0244 m/s.

This happens because at higher concentration of oil the granules get saturated quicker and therefore get heavier leading to greater elutriation. Therefore the bed height is reduced as shown in Figure 3.11. This is also found by looking at the pressure drop plots in Figure 3.12 which shows that the pressure drop of an inverse fluidized bed of aerogel granules facing higher concentration is less than the granules facing lower concentration of oil.

The effect of different superficial velocity of fluid entering the inverse fluidized bed of particles was also studies. In this experiment the operating conditions such as oil concentration, size of the granules, type of granules, and mass of the granules were kept the same.

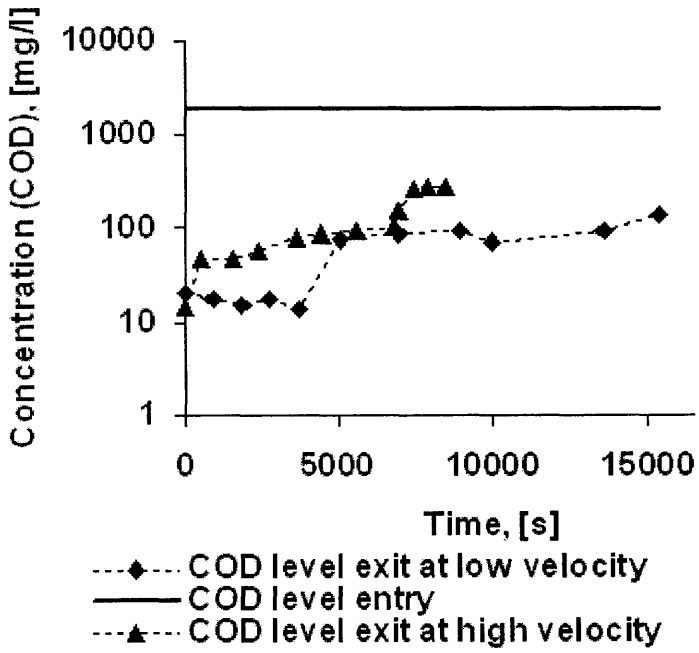

Figure 3.13 Chemical oxygen demand (COD) vs. time of 56 grams of aerogel granules (TLD 101) with sizes between 0.5 to 0.85 mm during removal of oil from water (0.45 g of oil/kg of water) at two different velocities of 0.0107 m/s (low velocity) and 0.0183 m/s (high velocity).

The Figure 3.13 shows the plots of the experimental runs done at two different velocities. Here the operating conditions were as follows. The fluid velocities were 0.011 and 0.018 m/s, the aerogel granules were TLD 101 (0.5 – 0.85 mm), and the mass of granules was 0.056 kg. According to this figure, the removal capacity of aerogel is higher when the superficial velocity of fluid is low. When the fluid velocity is low the void fraction of the bed is small; therefore the aerogel granules while absorbing oil on their surface can collide with each other and agglomerate. Due to the agglomeration of aerogel particles, the effective buoyancy increases and the particles do not get entrained by the fluid and stay in the fluidized bed to absorb more oil. Moreover, a high velocity may also lead to slight bypassing of the fluid through the fluidized bed would result in a lower oil removal efficiency.

One more experiment was conducted to see the effect of using different mass of granules in the inverse fluidized bed of aerogel. It was again found that using more granules means increasing the bed height which consequently increases the residence time of the oil droplets in the fluidized bed. Therefore, the removal capacity and the removal efficiency of the aerogel granules are higher when a greater mass of granules is used. The results of this experiment are shown in Figure 3.14 and the corresponding operating conditions employed were as follows. The fluid velocity was 0.010 m/s, the aerogel granule was TLD 101 (0.5 – 0.85 mm) and the inlet oil concentration was 0.45 kg of oil/kg of water.

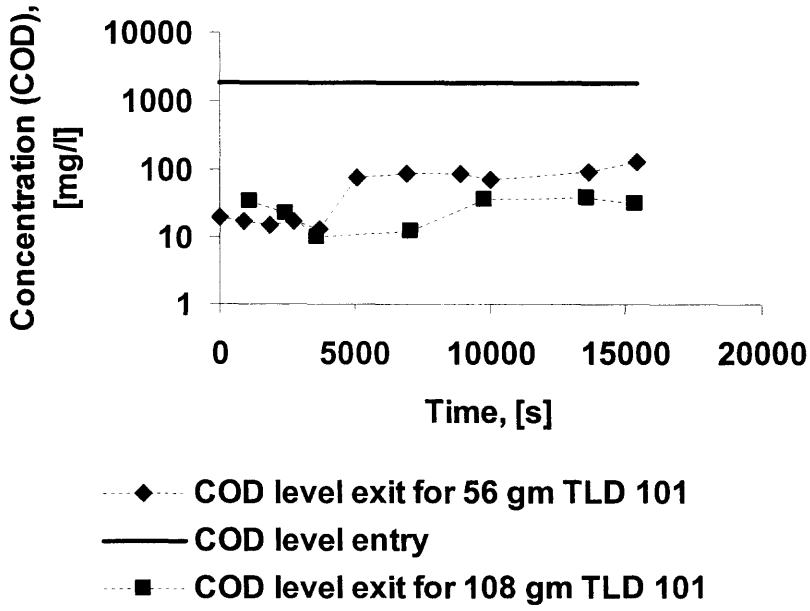

Figure 3.14 Chemical oxygen demand (COD) as a function of time of 108 grams and 56 grams of aerogel granules (TLD 101) with sizes between 0.5 to 0.85 mm during removal of oil from water (0.47 g of oil/kg of water and 0.0102 m/s fluid velocity).

The two different quantities of aerogel used were 0.056 kg and 0.108 kg. It is seen from the plots of Figure 3.14 that the downstream COD concentration for the experiment with the greater mass of aerogel reaches the value of 100 mg/l comparatively slower. This means that as more the aerogel is used, the removal efficiency is higher.

Another important experiment was conducted to compare the oil removal capacity and efficiency of two different sizes of TLD type aerogel granules. The two different sizes chosen were 0.5 – 0.85 mm and 1.7 - 2.3 mm.

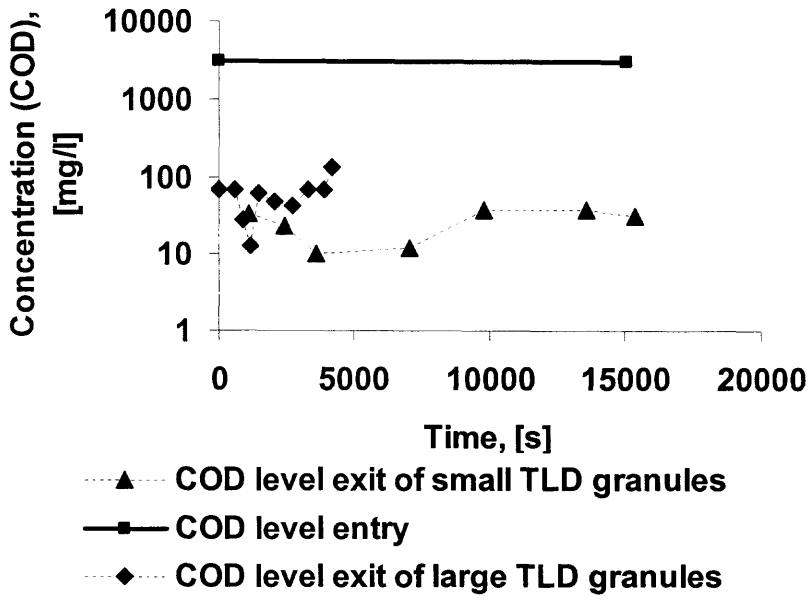

Figure 3.15 Chemical oxygen demand (COD) vs. time of 100 grams of aerogel granules (TLD 101) with sizes between 1.7 to 2.3 mm (large) and 0.5 – 0.85 mm (small) during removal of oil from water (0.4 g of oil/kg of water).

Figure 3.15 shows the COD concentration profile for both the sizes of granules used when inversely fluidizing them under the same operating conditions. The fluid velocity for TLD 101 (0.5 – 0.85 mm) granules was 0.01 m/s and the fluid velocity for TLD 302 (1.7 – 2.3 mm) granules was 0.035 m/s. The mass of the aerogel used in both cases was 0.1 kg and the upstream concentration of oil was 0.4 kg of oil/kg of water. By looking at the figure it is clear that when the smaller granules were used the COD levels remained below 100 mg/l for more than 3 hours, while the COD levels quickly reached the 100 mg/l concentration in 1 hour for the larger granules. Moreover, the figure also shows that the COD levels for the smaller granules remained as low as 40 mg/l while the COD levels for the larger granules were between 40 to 100 mg/l. This indicates that the oil removal efficiency of the smaller granules is higher than larger granules.

The US Coast Guard and the Maritime Spill Response Corporation after conducting joint tests to evaluate a number of separators listed in the World Catalog of Oil Spill Response Products, have suggested certain operating requirement list below for the oil spill recovery separators.

- The through put capacity should be in the range of 57 - 113 m^3/h.
- The weight of the separator should be in the range 1818 – 2727 kg.
- The volume occupied by the separator should be within 3.51 m^3.
- The Separator should be able to process oil in the viscosity range of 1500 – 50000 cSt.
- The effluent concentration of water should not be more than 15 ppm.

An inverse fluidized bed of Nanogel as described above could be one of the solutions for oil spill recovery operations if the capital and operating cost of this system are competitive with other available systems. Based on the experiments reported above, it appears that the inverse fluidized bed design can meet the requirements of the minimum required throughput, the maximum allowable weight and volume of the system and the maximum allowable effluent concentrations.

CHAPTER 4

CONCLUSIONS AND RECOMMENDATIONS FOR FUTURE STUDY

The results obtained from the oil removal experiments show that the inverse fluidized bed of ligher-than-water aerogel granules, like Nanogel®, can be an effective technique.

The results obtained from the inverse fluidization of Nanogel® could be summarized as follows. The fluidization was a typical smooth, particulate fluidization. Using appropriate equation and calculations, the granule density of the particles used in the fluidization experiments was found to be in the range 112 – 127 kg/m^3 and the bed void fraction was in the range of 0.4 – 0.5. The granule size calculated by using the Richardson and Zaki analysis, was in reasonable agreement with the assumed size of the granules based on sieving. The Richardson and Zaki exponent 'n' was found to be between 2.25 and 2.33. The terminal velocity of the smaller granules (0.5-0.85mm) was calculated to be between 0.04 to 0.05 m/s while the terminal velocity for larger granules (1.7 – 2.3mm) was between 0.15 to 0.17 m/s. The minimum fluidization velocity of smaller granules calculated from the Wen and Yu equation did not agree well with the experimental values. But, the Frantz correlation approximated the minimum fluidization velocity better than the Wen and Yu equation. Moreover, the Wen and Yu equation was reasonably good for approximating the minimum fluidization velocities of the larger granules (1.7 – 2.3mm).

The results obtained by using an IFB of aerogel granules for the removal of oil from water are summarized as follows. Smaller granules are more efficient in removing oil from water compared to larger granules. A lower fluid velocity leads to higher oil

removal capacity of aerogel granules. The oil removal capacity of an inverse fluidized bed of aerogel granules can be increased by increasing the amount of aerogel in the system. In other words, if the residence time of the oil droplets in the fluidized bed system is increased, a better removal efficiency and capacity can be obtained. The OGD 303 (dark) granules gave better results; this may be due to the fact that they are more porous and may have a larger surface area for the absorption of oil from water as compared to the same sized TLD 101 (translucent) granules.

The major advantage of an inverse fluidized bed are: an inverse fluidized bed offers higher flow rates at less pressure drop compared to packed bed filters. Due to low pressure drop, a larger amount of granules can be used in an inverse fluidized bed compared to a packed bed filter. Moreover, higher concentrations of oil can also be treated because as the granules get saturated, they become heavy thereby reducing the pressure drop of the bed, which is opposite to what is observed in a packed bed filter. The aerogel granules which are fragile can easily break down and produce fines when there is a high pressure drop as in a packed bed filter, whereas in an inverse fluidized bed due to low pressure drop and higher void fraction, the granules do not break at all. Since the aerogel granule density is as low as 100 kg/m^3, it is extremely light weight compared to its volume. Therefore the aerogel granules fluidized at a relatively high minimum fluidization velocity in an inverse fluidized bed. A higher minimum fluidization velocity means a higher throughput and the flowrate of water can be increased without having the problem of entrainment of particles. This means a larger volume of contaminated water can be treated. Moreover, the inverse fluidized bed of Nanogel has an advantage over the

presently used inverse fluidized bed bio-reactors because the former eliminates the problem of contamination of water by the micro-organisms.

The major conclusion from the results presented in this thesis is that an inverse fluidized bed of aerogels is a novel and effective method to remove oil from wastewater. Although a number of experiments were carried out as a proof of concept, much more research has to be done regarding many aspects of this operation. More data needs to be generated to collect information on the effect of the size of the granules, the superficial velocity of the oil-water mixture, the diameter and height of the column of granules, the range of concentration of oil entering the column and the range of operable pressure drop for the system. Moreover, more work is required to determine if an IFB can be used for the removal of other contaminants of water such as unwanted minerals, heavy metals and other hydrocarbons which are either soluble or insoluble in water. Other low density, hydrophobic, highly porous particles should be tested in the inverse fluidized bed system and compared to the aerogels with regard to oil removal efficiency, pressure drop and capacity. Particle characterization using a scanning electron microscope (SEM) and/or a transmission electron microscope (TEM) should also be done to compare the structure of the aerogel particles before and after the absorption of oil. After obtaining the experimental data, a predictive mathematical model should be developed and computer simulations performed to allow for the design, optimization and scale up of an industrial-sized system.

REFERENCES

Ayres, M., Hunt, A. Silica Aerogels. (http://eetd.lbl.gov/ECS/aerogels/satoc.htm) Retrieved September 20, 2006 from the World Wide Web.

Alsaigh, R., Boerma, J., Ploof, A., Regenmorter, L., 1999. Evaluation of On-line Media Filters in the Rouge River Watershed. Rouge River National Wet Weather Demonstration Project. Nonpoint work plan No. URBSW5, Task No. 3. (http://www.rougeriver.com//pdfs/stormwater/tpm59.pdf). Retrieved September 29, 2006.

Bendict, F. R. J., Kumaresan, G., Velan, M., 1998. Bed Expansion and Pressure Drop Studies in a Liquid-solid Inverse-fluidised Bed Reactor. Bioprocess Engineering 19, 137-142.

Cambiella, A., Ortea, E., Rios, G., Benito, J. M., Pazos, C., Coca, J., 2006. Treatment of Oil-in-water Emulsions: Performance of a Sawdust Bed Filter. Journal of Hazardous Materials B131, 195-199.

Cho, Y. J., Park, H. Y., Kim, S. W., Kang, Y., Kim, S. D., 2002. Heat Transfer and Hydrodynamics in Two-and Three-Phase Inverse Fluidized Beds. Industrial and Engineering Chemistry Research 41, 2058-2063.

EPA US., 2006. Sorbent Materials in Storm Water Applications. Retrieved October 9, 2006 from the World Wide Web: *http://epa.gov/owm/mtb/sorbmat.pdf*.

EPA US., 1999. The Pollution Prevention Tool Kit, Best Environmental Practices for Fleet Maintenance. Publication number EPA-909-E-99-001.

Fan, L. S., Muroyama, K., Chern, S. H., 1982. Hydrodynamic Characteristics of Inverse Fluidization in Liquid-Solid and Gas-Liquid-Solid Systems. The Chemical Engineering Journal 24, 143-150.

Furrow, B. E., 2005. Analysis of Hydrocarbon Removal Methods for the Management of Oilfield Brines and Produced Waters. MS Thesis, Texas A & M University, Texas.

Gaaseidnes, K., Turbeville, J., 1999. Separation of Oil and Water in Oil Spill Recovery Operations. Pure and Applied Chemistry 71(1), 95-101.

Garcia-Calderon, D., Buffiere, P., Moletta, R., Elmaleh, S., 1998. Influence of Biomass Accumulation on Bed Expansion Characteristics of a Down-Flow Anaerobic Fluidized-Bed Reactor. Biotechnology and Bioengineering 57(2), 136-144.

Goldsmith, R., Hossian, S., 1973. Ultrafiltration Concept for Separating Oil from Water. Washington: U.S. Coast Guard.

Gupta, C.K., Sathiyamoorthy, D., 1999. Fluid Bed Technology in Materials Processing. CRC Press.

Hach Co. Method 8000: Reactor digestion method USEPA approved for oxygen chemical demand wastewater analysis., 2004. DR/890 Datalogging Colorimeter Handbook, 427-436.

Hayes, T., Arthur, D., 2004. Overview of Emerging Produced Water Treatment Technologies. The 11th Annual International Petroleum Environmental Conference, 1-19.

Hrubesh, L.W., Coronado, P.R., Dow, J.P., 2004. Method for Removing Organic Liquids from Aqueous Solutions and Mixtures. U.S. Patent 6709600 , 2004.

Ibrahim, Y. A. A., Briens, C. L., Margaritis, A., Bergongnou, M. A., 1996. Hydrodynamic Characteristics of a Three-Phase Inverse Fluidized-Bed Column. AIChE Journal 42(7), 1889-1900.

Jirka, A. M., Carter, M. J., 1975. Reactor Digestion Method for COD Analysis. Analytical Chemistry 47(8), 1397.

Johnson, R. F., Manjrekar, T. G., Halligan, H. R., 1973. Removal of Oil from Water Surfaces by Sorption on Unstructured Fibers. Environmental Science and Technology 7, 439-443.

Karamanev, D. G., Nikolov, L. N., 1992. Bed Expansion of Liquid-Solid Inverse Fluidization. AIChE Journal 38(12), 1916-1922.

Lee, D. H., Epstein, N., Grace, J. R., 2000. Hydrodynamic Transition from Fixed to Fully Fluidized Beds for Three-phase Inverse Fluidization. Korean Journal of Chemical Engineering 17(6), 684-690.

Manning, F., Snider, E. H., 1983. Assesment Data Base for Petroleum Refining Wastewater and Residues. Washington: U.S. department of Commerce, NTIS, 94-101.

Manual on Disposal of Refining Wastes., 1969. American Petroleum Institute, 5, 5-15.

Mathavan, G. N., Viraraghavan, T., 1989. Use of Peat in the Treatment of Oily Waters. Water, Air, and Soil Pollution 45, 17-26.

Mysore, D., Viraraghavan, T., Jin, Y. C., 2006. Vermiculite Filtration for Removal of Oil from Water. Practice Periodical of Hazardous, Toxic, and Radioactive Waste Management, 156-161.

National Conference on Urban Runoff Management: Enhancing Urban Watershed Management at the Local, County, and State Levels, USA., 1993. Training for Construction Site erosion Control and Stormwater Facility Inspection.

Nikov, I., Karamanev, D., 1991. Liquid-Solid Mass Transfer in Inverse Fluidized Bed. AICHE Journal 37(5), 781-784.

Pasila, A., 2004. A Biological Oil Adsorption Filter. Marine Pollution Bulletin 49, 1006-1012.

Paterson, J. W., 1985. Industrial Wastewater Treatment Technology. Butterworth Publishers, Inc. 2nd Edition, Stoneham, MA.

Quemeneur, M., Marty, Y., 1994. Fatty Acids and Sterols in Domestic Wastewaters. Water Research 28, 1217-1226.

Renganathan, T., Krishnaiah, K., 2003. Prediction of Minimum Fluidization Velocity in Two and Three Phase Inverse Fluidized Beds. The Canadian Journal of Chemical Engineering 81, 853-860.

Renganathan, T., Krishnaiah, K., 2004. Liquid Phase Mixing in 2-phase Liquid-solid Inverse Fluidized Bed. Chemical Engineering Journal 98, 213-218.

Renganathan, T., Krishnaiah, K., 2004. Stochastic Simulation of Hydrodynamics of a Liquid-Solid Inverse Fluidized Bed. Industrial Engineering Chemistry Research 43, 4405-4412.

Renganathan, T., Krishnaiah, K., 2005. Voidage Characteristics and Prediction of Bed Expansion in Liquid-solid Inverse Fluidized Bed. Chemical Engineering Science 60, 2545-2555.

Ribeiro, T. H, Rubio, J., Smith, R. W., 2003. A Dried Hydrophobic Aquaphyte as an Oil Filter for Oil/Water Emulsions. Spill Science & Technology Bulletin 8(5-6), 483-489.

Richardson, J. F., Zaki, W. N., 1954. Sedimentation and Fluidization: Part I. Transaction of the Institution of Chemical Engineers 32, 35-53.

Sakiadis, B. C., 1984. Fluid and Particle Mechanics. Perry's Chemical Engineer's Handbook.

Smirnova, I., 2002. Synthesis of silica aerogels and their application as a drug delivery system. PhD Thesis, Technical University of Berlin, Berlin, Germany.

Stenstrom, M. K., Lau, S-L., 1998. Oil and Grease Removal by Floating Sorbent in a CDS Device. CDS Technologies, Los Angeles.

Wen, C. Y., Yu, Y. H., 1966. Mechanics of Fluidization. Chemical Engineering Progress Symposium Series 62(2), 100.